CORE
Metadata, citation and similar papers at core.ac.uk
Provided by RERO DOC Digital Library

The Grønnedal-Ika Carbonatite–Syenite Complex, South Greenland: Carbonatite Formation by Liquid Immiscibility

RALF HALAMA[1,*], TORSTEN VENNEMANN[2], WOLFGANG SIEBEL[1] AND GREGOR MARKL[1,†]

[1]INSTITUT FÜR GEOWISSENSCHAFTEN, EBERHARD-KARLS-UNIVERSITÄT TÜBINGEN, WILHELMSTRASSE 56, D-72074,TÜBINGEN, GERMANY

[2]INSTITUT DE MINÉRALOGIE ET GÉOCHIMIE, UNIVERSITÉ DE LAUSANNE, UNIL-BFSH2, CH-1015 LAUSANNE, SWITZERLAND

RECEIVED NOVEMBER 6, 2003; ACCEPTED AUGUST 2, 2004
ADVANCE ACCESS PUBLICATION SEPTEMBER 9, 2004

The Grønnedal-Ika complex is dominated by layered nepheline syenites which were intruded by a xenolithic syenite and a central plug of calcite to calcite–siderite carbonatite. Aegirine–augite, alkali feldspar and nepheline are the major mineral phases in the syenites, along with rare calcite. Temperatures of 680–910°C and silica activities of 0·28–0·43 were determined for the crystallization of the syenites on the basis of mineral equilibria. Oxygen fugacities, estimated using titanomagnetite compositions, were between 2 and 5 log units above the fayalite–magnetite–quartz buffer during the magmatic stage. Chondrite-normalized REE patterns of magmatic calcite in both carbonatites and syenites are characterized by REE enrichment (La_{CN}–Yb_{CN} = 10–70). Calcite from the carbonatites has higher Ba (~5490 ppm) and lower HREE concentrations than calcite from the syenites (54–106 ppm Ba). This is consistent with the behavior of these elements during separation of immiscible silicate–carbonate liquid pairs. $\varepsilon_{Nd}(T = 1{\cdot}30\,Ga)$ values of clinopyroxenes from the syenites vary between +1·8 and +2·8, and $\varepsilon_{Nd}(T)$ values of whole-rock carbonatites range from +2·4 to +2·8. Calcite from the carbonatites has $\delta^{18}O$ values of 7·8 to 8·6‰ and $\delta^{13}C$ values of −3·9 to −4·6‰. $\delta^{18}O$ values of clinopyroxene separates from the nepheline syenites range between 4·2 and 4·9‰. The average oxygen isotopic composition of the nepheline syenitic melt was calculated based on known rock–water and mineral–water isotope fractionation to be 5·7 ± 0·4‰. Nd and C–O isotope compositions are typical for mantle-derived rocks and do not indicate significant crustal assimilation for either syenite or carbonatite magmas. The difference in $\delta^{18}O$ between calculated syenitic melts and carbonatites, and the overlap in ε_{Nd} values between carbonatites and syenites, are consistent with derivation of the carbonatites from the syenites via liquid immiscibility.

KEY WORDS: *alkaline magmatism; carbonatite; Gardar Province; liquid immiscibility; nepheline syenite*

INTRODUCTION

Carbonatites typically occur in close association with alkaline silicate igneous rocks, either in individual complexes or in a regional association within particular magmatic provinces (e.g. Harmer, 1999). However, the genetic relationship between carbonatites and associated silicate rocks is complex and not completely understood (e.g. Bell, 1998; Bell *et al.*, 1998). Proposed models for the generation of carbonatites include direct melting of a carbonate-bearing mantle source (e.g. Wyllie & Huang, 1976; Dalton & Presnall, 1998; Harmer & Gittins, 1998; Moore & Wood, 1998), derivation by immiscible separation from a carbonated silicate melt (e.g. Koster van Groos & Wyllie, 1973; Freestone & Hamilton, 1980; Kjarsgaard & Hamilton 1988; Brooker, 1998; Kjarsgaard, 1998) and crystal fractionation of a carbonated alkali silicate melt (e.g. Lee & Wyllie, 1994; Korobeinikov *et al.*, 1998; Veksler *et al.*, 1998*a*). There is, however, still a lack of robust criteria that can be

*Present address: Institut de Physique du Globe de Paris, Case courrier 109, 4 Pl. Jussieu, 75005 Paris, France.
†Corresponding author. Telephone (+49) 7071/2972930. Fax: (+49) 7071/293060. E-mail: markl@uni-tuebingen.de

 © Oxford University Press 2004; all rights reserved

used to distinguish carbonatitic melts directly derived from the mantle from those produced by differentiation of a parent silicate melt (Bell, 1998).

This study explores geochemical and petrological data from the mid-Proterozoic Grønnedal-Ika nepheline syenite–carbonatite complex in the Gardar Province, South Greenland. The complex represents the most significant occurrence of carbonatite in the province. It is well suited to study the relationship between carbonatite and associated silicate rocks because the carbonatite occurs in close spatial association with nepheline syenitic rocks. Previous studies of Grønnedal-Ika investigated the petrography, whole-rock geochemistry and mineral chemistry of the complex (Emeleus, 1964; Bedford, 1989; Goodenough, 1997; Pearce *et al.*, 1997). In this study, we focus on new O and Nd isotope data from minerals of the syenites combined with Nd isotope data from the carbonatite to address still open questions about liquid immiscibility. *In situ* trace-element data from minerals are used to evaluate the constraints given by experimental and theoretical carbonate liquid–silicate liquid partitioning data. Additionally, the petrological and geochemical characteristics of the syenites are compared with other syenitic complexes in the province in order to explore differences in terms of magma evolution that can be related to carbonatite formation.

PREVIOUS WORK AND GEOLOGICAL SETTING

The first detailed account of the Grønnedal-Ika complex was given by Callisen (1943), who established the intrusive character of the alkaline rocks. Emeleus (1964) reconstructed the history of the complex based on detailed mapping and petrographic observations. Later, Gill (1972*a*, 1972*b*) and Bedford (1989) obtained numerous geochemical data on minerals and whole rocks from the complex and associated phonolite dykes. C, O and Sr and a few Nd whole-rock isotopic data were obtained by Goodenough (1997), Pearce *et al.* (1997) and Coulson *et al.* (2003).

The Grønnedal-Ika complex (Fig. 1a) is 8 km × 3 km in exposed dimension and consists predominantly of layered nepheline syenites, which were intruded by a xenolithic porphyritic syenite and a plug of carbonatite (Emeleus, 1964). It was emplaced into the border zone between the Julianehåb batholith (1850–1800 Ma; Garde *et al.*, 2002), which is part of the Ketilidian mobile belt to the south and the Archean block to the north (Fig. 1b). The country rocks comprise quartzo-feldspathic gneisses, occasional amphibolites and rare calc-silicates (Bedford, 1989). The complex was dated at 1299 ± 17 Ma by Rb–Sr (Blaxland *et al.*, 1978). This age is consistent with field observations indicating that it pre-dates emplacement of a suite of olivine dolerite dykes ('Brown Dikes') for which an U–Pb age of 1280 ± 5 Ma has been determined (Upton *et al.*, 2003). The layered and laminated syenites are considered to have formed mainly by consolidated by bottom accumulation and adhesion to steep-sided cooling surfaces (Emeleus, 1964). The original structure of the complex comprises two series of layered syenites—the Lower Series and the Upper Series, which are separated by a raft of gneiss (Emeleus, 1964). Several distinct intrusive phases can be distinguished, but gradational relationships between different rock types within intrusive units are common (Callisen, 1943; Emeleus, 1964). For a detailed description of the syenitic rocks from Grønnedal-Ika, the reader is referred to the previous studies of Emeleus (1964) and Bedford (1989). For the purpose of this study, the Upper and Lower Series syenites are combined as the Layered Syenites (LS). At one locality in the Lower Series syenites, some 20 gabbroic xenoliths, roughly 5–30 cm in diameter, were found. Porphyritic microsyenites (PMS) occur as dykes and sheets, and cut across earlier units of the complex. A xenolithic porphyritic syenite (XPS) is the youngest of the intrusive syenites. It contains abundant xenoliths of earlier syenites, trachytes, gneisses and amphibolites. Finally, a central plug of calciocarbonatite was emplaced into the syenites (Emeleus, 1964; Pearce *et al.*, 1997). There are three major and several smaller outcrops of carbonatite that are thought to have belonged to one central plug (Emeleus, 1964). The carbonatite is xenolithic with fragments of syenites and other rocks. It consists essentially of varying amounts of calcite, siderite and magnetite; calcite is dominant. Towards the centre of the carbonatite plug, the amount of siderite increases. Large amounts of magnetite occur where mafic dykes cut the siderite-rich part of the carbonatite (Emeleus, 1964). The syenites in close contact with the carbonatite are altered and impregnated by calcite. Sodalite and sodalite ± calcite veins occur in various units of the complex. There is no field evidence for a significant time-gap between the emplacement of the syenites and the carbonatite. The last stage of magmatic activity, at about 1280 Ma, is represented by the intrusion of a variety of dykes, including lamprophyres, porphyritic dolerites and several olivine dolerites up to a few tens of meters wide. Trachytic, phonolitic and other alkaline dykes were emplaced during renewed magmatic activity during later Gardar (~1250–1150 Ma) times. Intense faulting, responsible for the elongated outline of the complex, took place largely following, but in part contemporaneous with, the intrusion of these dikes (Emeleus, 1964).

Mainly on the basis of whole-rock REE and other trace-element data, Bedford (1989) proposed an origin for the Grønnedal-Ika carbonatites via liquid immiscibility from a nepheline syenitic liquid. He envisaged that the XPS represents the conjugate

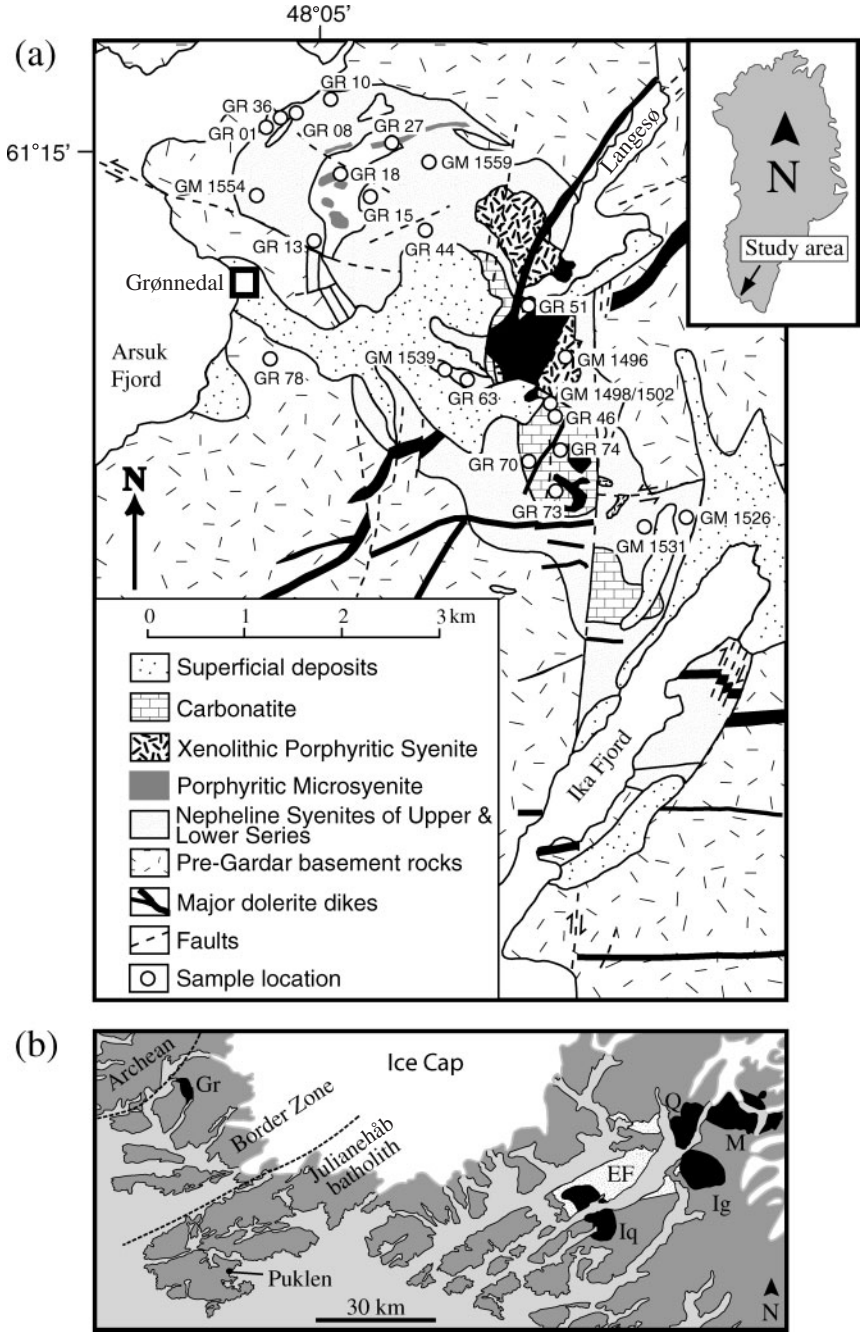

Fig. 1. (a) Map of the Grønnedal-Ika intrusion, simplified after Emeleus (1964) and Pearce *et al.* (1997). (b) Simplified map after Upton *et al.* (2003) showing the boundaries between the main tectonic units (dashed lines) and the locations of Gardar rocks referred to throughout the text (igneous complexes are shown in black, the volcano-sedimentary Eriksfjord Formation with a dotted pattern). Gr, Grønnedal-Ika; Ig, Igdlerfigssalik; Iq, Ilímaussaq; M, Motzfeldt; Q, North and South Qôroq; EF, Eriksfjord Formation.

silicate liquid to the carbonatite. However, Pearce *et al.* (1997) concluded that the syenites and carbonatites are unrelated because of differences in their C and O isotopic compositions. They presented data suggesting that the carbonatites are, instead, linked to lamprophyre dikes. The spatial association of carbonatites and lamprophyres is a common feature in the Gardar Province, and a general genetic link between them has been proposed previously (Coulson *et al.*, 2003). The data presented in this study are used to re-evaluate the controversy, and a particular focus is given to the XPS as a critical unit of the complex.

ANALYTICAL METHODS

Electron microprobe analysis

Mineral compositions were determined using a JEOL 8900 electron microprobe (EMP) at the Institut für Geowissenschaften, Universität Tübingen, Germany. An internal φρz correction of the raw data was applied (Armstrong, 1991). Both natural and synthetic standards were used for major and minor elements. Measuring times were 16 and 30 s on the peak positions for major and minor elements, respectively. The emission current was 15 nA and the acceleration voltage 15 kV. For nepheline analyses, a beam diameter of 5 μm was used to avoid errors resulting from diffusion of Na. Feldspars with microperthitic exsolution were measured with a 20 μm wide beam and an average of 2–4 analyses was taken as representative for the respective grain. The bulk compositions of oxy-exsolved titanomagnetite grains were reconstructed by combining image-processed (NIH Image software) back-scattered electron images of the exsolved grains and point analyses of exsolved ilmenite and magnetite according to the method described by Marks & Markl (2001).

Laser ICP–MS *in situ* trace-element measurements

In situ laser ablation inductively coupled plasma–mass spectrometry (LA-ICP–MS) analyses on ~150 μm thick polished sections were performed at the EU Large-Scale Geochemical Facility (University of Bristol) using a VG Elemental PlasmaQuad 3 + S-Option ICP–MS system equipped with a 266 nm Nd–YAG laser (VG MicroProbe II). The laser beam diameter at the sample surface was approximately 20 μm. Analyses of calcite were carried out in a beam rastering mode, as ablation of calcite was rapid. Details of the data acquisition have been described elsewhere (Halama *et al.*, 2002). The precision of trace-element concentrations, based on repeated analyses of NIST 610 and 612 glass standards, is approximately ±5% for element concentrations >10 ppm and ±10% for concentrations <10 ppm. Typical detection limits for most trace elements in this study were 0·1–1 ppm, except for Sc, Co and Zn, with detection limits in the range of 1–5 ppm. For the REE, detection limits were generally <0·5 ppm.

Oxygen and carbon isotope analysis

The oxygen isotope composition of hand-picked clinopyroxene separates was measured using a method similar to that described by Sharp (1990) and Rumble & Hoering (1994). Hand-picked clinopyroxene (1–2 mg) was loaded onto a Pt-sample holder. The sample chamber was pumped to a vacuum of about 10^{-6} mbar and pre-fluorinated overnight. Samples were then heated with a CO_2 laser in an atmosphere of 50 mbar of pure F_2. Excess F_2 was separated from O_2 by conversion to Cl_2 using KCl held at 150°C and the extracted O_2 was collected on a molecular sieve (13X). Oxygen isotopic compositions were measured on a Finnigan MAT 252 mass spectrometer at the Institut für Geowissenschaften, Universität Tübingen. The results are reported as the ‰ deviation from Vienna Standard Mean Ocean Water (V-SMOW) in the standard δ-notation. Replicate analyses of the NBS-28 quartz standard yielded an average precision of ±0·1‰ (1σ) for $\delta^{18}O$ values. In each run, standards were analyzed at the beginning and the end of the sample set. A correction, generally <0·3‰, was then applied to the data, equal to the average difference between the mean measured value and the accepted value for the standard of 9·64‰.

The carbon and oxygen isotope compositions of the carbonates were measured in automated mode using a GasBench from ThermoFinnigan connected directly to a Finnigan MAT 252 mass spectrometer. The method has been described in detail by Spötl & Vennemann (2003). About 200–400 μg of sample material was recovered as powder by micro-drilling into the calcite. CO_2 was obtained by reaction of the sample with several drops of 100% orthophosphoric acid and was carried via a He stream over traps to remove water vapor and a gas chromatograph-column to separate CO_2 from possible interfering gases before being passed into the mass spectrometer for isotopic analysis. The C and O isotope compositions are reported in the standard δ-notation, relative to PDB and V-SMOW, respectively; standard analytical errors are ±0·1‰ (1σ) for both $\delta^{13}C$ and $\delta^{18}O$.

Nd isotope analysis

For Nd isotope analyses, 15–20 mg of hand-picked clinopyroxene from the same separates used for the O analysis, and 5–8 and 40 mg of whole-rock powder of carbonatite and basement samples, respectively, were used. Details of the analytical procedures have been described elsewhere (Halama *et al.*, 2003). $^{143}Nd/^{144}Nd$ ratios were normalized for mass fractionation to $^{146}Nd/^{144}Nd = 0{\cdot}7219$. The average $^{143}Nd/^{144}Nd$ ratio obtained for the Ames Nd-standard (Roddick *et al.*, 1992) was 0·512119 ± 10 (1σ, $n = 42$) during the course of this study, and the La Jolla Nd standard gave 0·511831 ± 30 (1σ, $n = 12$). The total procedural blank (chemistry and loading) was <100 pg for Nd.

PETROGRAPHY AND MINERAL CHEMISTRY

Syenites

The major mafic silicate in the Layered Syenites is euhedral to subhedral or poikilitic clinopyroxene (Fig. 2a–c).

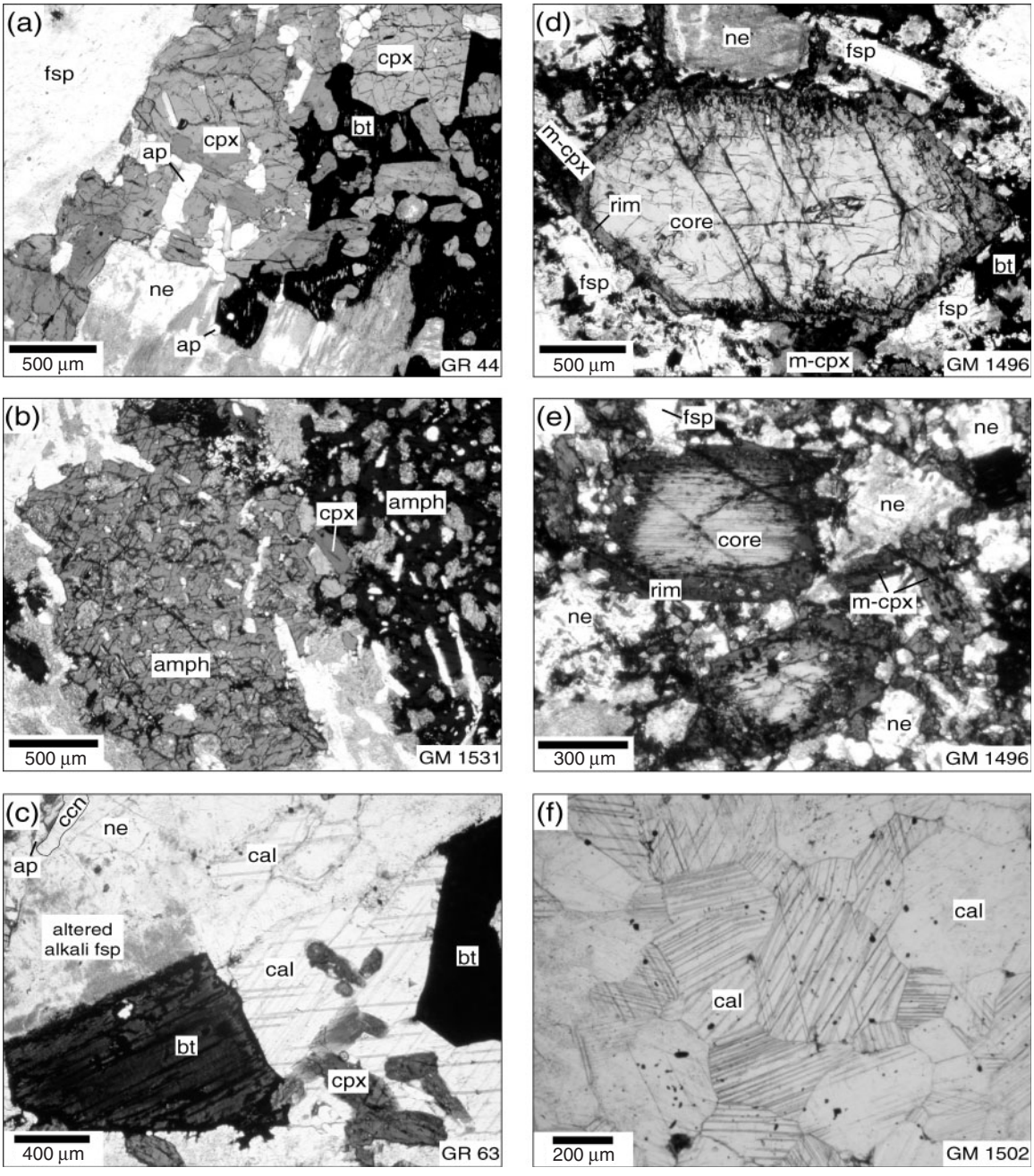

Fig. 2. Photomicrographs (plane-polarized light) of mineral textures from the Grønnedal-Ika rocks. Sample numbers appear in the lower right corner. Ne, nepheline; fsp, alkali feldspar; cpx, clinopyroxene; m-cpx, matrix clinopyroxene; bt, biotite; amph, amphibole; ap, apatite; cal, calcite; ccn, cancrinite. (a) Typical texture of the layered nepheline syenites with an accumulation of clinopyroxene, partly surrounded by biotite and with associated apatite; (b) large, poikilitic amphibole; (c) interstitial calcite among biotite, clinopyroxene and alkali feldspar; the boundaries of the cancrinite in the upper left corner are have been outlined to increase its visibility; (d) and (e) clinopyroxene phenocrysts in the XPS showing discontinuous zonation from core to rim, together with small matrix clinopyroxenes; alkali feldspar and nepheline occur as phenocrysts and within the matrix; (f) calcite grains in calcite carbonatite.

Clinopyroxenes are typically cumulus phases and commonly rimmed by intercumulus biotite. Most clinopyroxenes can be classified as aegirine–augites (Morimoto *et al.*, 1988), but diopsidic pyroxene and aegirine occur occasionally. Typical clinopyroxene compositions are summarized in Table 1 and compositional trends are shown in Fig. 3a–c. In some samples, clinopyroxene shows a weak, patchy zonation with limited compositional

Table 1: Representative single spot electron microprobe analyses of clinopyroxene from the Grønnedal-Ika syenites

Unit:	LS	LS	LS	LS	LS	LS	LS	XPS	XPS	PMS	PMS	GX
Sample:	GR 01	GR 36	GR 36	GM 1526	GR 63	GM 1531	GM 1559	GR 51	GR 51	GR 27	GR 27	GR 08
Mineral:	Cpx	Cpx	Cpx	Cpx	Cpx	Cpx	Cpx	Cpx (core)	Cpx (rim)	Cpx	Cpx	Cpx
wt %												
SiO_2	51·44	50·12	52·10	51·68	51·30	51·30	50·82	48·94	50·86	50·11	49·97	50·77
TiO_2	0·20	0·68	0·43	0·19	0·17	0·28	0·19	1·41	0·33	0·22	0·09	1·02
Al_2O_3	1·18	2·96	0·76	0·86	1·10	1·11	1·23	4·45	0·85	1·33	1·07	2·50
FeO	25·50	13·48	27·51	23·00	21·42	26·44	19·24	12·43	23·98	20·72	24·91	11·82
MnO	0·78	0·36	0·33	0·79	0·96	0·55	0·87	0·24	0·84	0·84	0·92	0·26
MgO	1·39	9·78	0·67	3·31	4·09	0·84	5·41	9·20	2·43	4·75	2·00	11·23
CaO	12·55	21·18	7·59	14·24	16·14	9·13	17·63	20·96	13·19	20·25	16·06	21·52
Na_2O	6·36	1·08	9·77	5·59	4·35	8·41	3·63	1·79	6·43	1·93	4·40	0·88
K_2O	0·01	0·01	0·00	0·00	0·00	0·00	0·01	0·02	0·01	0·01	0·00	0·00
Total	99·40	99·65	99·16	99·68	99·54	98·06	99·04	99·44	98·92	100·17	99·42	100·00
Formulae based on 4 cations and 6 oxygens												
Si	2·00	1·91	1·99	1·99	1·99	2·00	1·97	1·86	1·97	1·96	1·97	1·91
Al	0·05	0·13	0·03	0·04	0·05	0·05	0·06	0·20	0·04	0·06	0·05	0·11
Ti	0·01	0·02	0·01	0·01	0·00	0·01	0·01	0·04	0·01	0·01	0·00	0·03
Fe^{3+}	0·41	0·09	0·68	0·38	0·29	0·57	0·27	0·14	0·48	0·16	0·35	0·07
Mg	0·08	0·56	0·04	0·19	0·24	0·05	0·31	0·52	0·14	0·28	0·12	0·63
Fe^{2+}	0·42	0·34	0·20	0·36	0·40	0·29	0·36	0·25	0·30	0·52	0·47	0·31
Mn	0·03	0·01	0·01	0·03	0·03	0·02	0·03	0·01	0·03	0·03	0·03	0·01
Ca	0·52	0·86	0·31	0·59	0·67	0·38	0·73	0·85	0·55	0·85	0·68	0·87
Na	0·48	0·08	0·72	0·42	0·33	0·63	0·27	0·13	0·48	0·15	0·34	0·06
K	0·00	0·00	0·00	0·00	0·00	0·00	0·00	0·00	0·00	0·00	0·00	0·00
Total	4·00	4·00	4·00	4·00	4·00	4·00	4·00	4·00	4·00	4·00	4·00	4·00
Di	8·0	56·5	3·9	19·2	23·7	4·9	32·2	57·1	14·8	28·5	12·3	62·5
Hed	44·2	35·4	21·4	38·7	43·5	31·0	39·6	28·4	34·3	56·4	52·6	31·2
Aeg	47·8	8·1	74·7	42·1	32·8	64·1	28·1	14·5	50·9	15·1	35·1	6·3

LS, Layered Syenites; GX, Gabbroic xenolith. Calculation of clinopyroxene end-members: Di = Mg, Hed = Fe^{2+} + Mn, Aeg = Na.

variability. Other samples contain clinopyroxenes with a marked growth zonation, with a compositional range in a single crystal as large as that in the entire sample suite. Compositions vary between $Di_{56}Hed_{34}Aeg_{10}$ and $Di_3Hed_2Aeg_{95}$. In comparison with compositional trends from other alkaline complexes of the Gardar Province (Fig. 3d), the extreme enrichment in Fe^{2+} at low values of Na, as seen in Ilímaussaq (Larsen, 1976) and Igdlerfigssalik (Powell, 1978), is lacking in Grønnedal. Clinopyroxene compositions in a gabbroic xenolith show a small range of $Di_{65–59}Hed_{30–36}Aeg_5$.

In the XPS, clinopyroxene phenocrysts reach up to 2 mm in length and show a marked discontinuous zoning, whereas matrix clinopyroxene grains are considerably smaller (<200 μm) and optically unzoned (Figs 2d and e, and 4a and b). The clinopyroxene phenocrysts in the XPS are characterized by a relatively Mg-rich core, overgrown by a distinctly more Na- and Fe^{3+}-rich rim with a compositional gap between (Fig. 3c). The most primitive core compositions in the XPS reach values of $Di_{57}Hed_{29}Aeg_{14}$, whereas the most evolved rims are $Di_7Hed_{22}Aeg_{71}$. Matrix clinopyroxene compositions in the XPS overlap with the more evolved phenocryst rim compositions.

Olivine is completely absent from the samples studied, but scarce relics of Fe-rich olivine have been observed (Emeleus, personal communication). Amphiboles are also scarce (Bedford, 1989), but they occasionally occur as poikilitic or subhedral intercumulus grains. Only one sample (GM 1531) was investigated in which poikilitic amphibole with a katophorite composition is the dominant mafic silicate phase (Fig. 2b). Biotite, usually

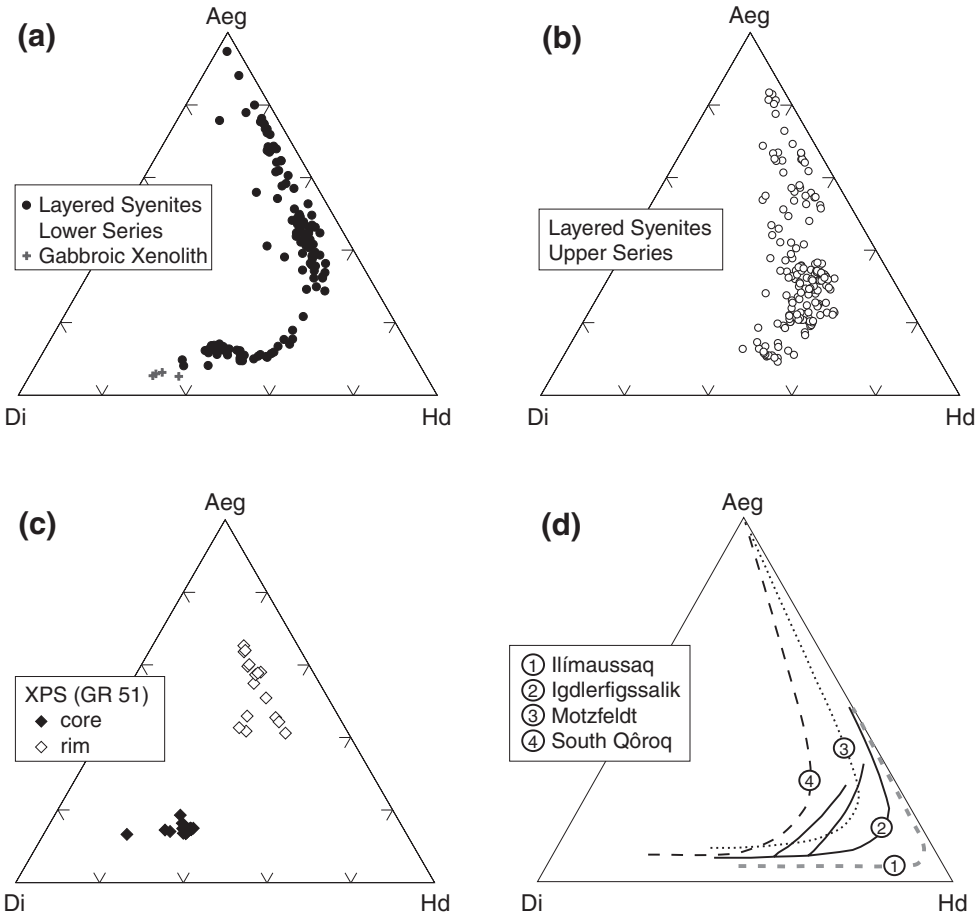

Fig. 3. (a)–(c) Compositions of clinopyroxenes from Grønnedal-Ika syenites in the diopside–hedenbergite–aegirine (Di–Hd–Aeg) triangle. End-member components were calculated as follows: Di = Mg, Hd = Fe^{2+} + Mn and Aeg = Na. (a) and (b) show compositions from the Layered Syenites; (c) core and rim compositions from a typical clinopyroxene of the XPS; (d) generalized trends of pyroxene compositions from other alkaline igneous complexes of the Gardar Province (1–4). Data sources: (1) Larsen (1976); (2) Powell (1978); (3) Jones (1984); (4) Stephenson (1973).

as intercumulus grains (Fig. 2a), occurs frequently and is often associated with hematite. All syenites from the Grønnedal-Ika complex are nepheline-bearing (Emeleus, 1964), and nepheline usually occurs as euhedral prisms (Fig. 2a–c). Nepheline is chemically unzoned and its composition is fairly homogeneous within individual samples and also within the whole sample suite, including the PMS and the XPS (Table 2). There are also no significant compositional differences between phenocrysts and matrix nepheline. The compositional variability spans the range $Ne_{73–68}Ks_{20–15}Qz_{7–16}$. The FeO and CaO contents of nepheline in all rock types are invariably <1 and <0·1 wt %, respectively. Nepheline is often replaced by the alteration products 'gieseckite' (fibrous, micaceous aggregates) and cancrinite (Fig. 2c). Cancrinite also occurs as individual grains, partly with poikilitic character suggestive of an intercumulus origin.

The abundant platy crystals of alkali feldspar frequently show perthitic exsolution into almost pure albite and orthoclase. Alkali feldspar phenocrysts of up to 1 cm in length occur in both the PMS and the XPS (Fig. 2d). Some samples contain feldspar with exsolution on a μm scale, so that the original bulk composition could be obtained using a defocused beam (Table 2). These bulk compositions are fairly homogeneous throughout the different rock types and vary in the range $An_{0–1}Ab_{39–54}Or_{46–60}$.

Primary magmatic titanomagnetite is relatively rare and characterized by a trellis-type oxy-exsolution texture [terminology after Buddington & Lindsley (1964)] of magnetite with lamellae of the hematite–ilmenite–pyrophanite solid solution series (Fig. 4c and d). The compositional variation in the lamellae ($Ilm_5Pyr_{93}Hem_2$–$Ilm_{56}Pyr_{23}Hem_{21}$) is in contrast to the constant composition of the magnetite ($Mag_{98–99}Usp_{1–2}$). Reintegrated oxide compositions vary from $Mag_{61}Usp_{39}$ to $Mag_{72}Usp_{28}$ (Table 3). This range reflects the chemical variability in the lamellae and is considered to cover fairly

Table 2: Representative microprobe analyses of feldspar and nepheline in Grønnedal-Ika syenites

Unit:	LS, Upper Series	LS, Upper Series	PMS	XPS	XPS	LS, Lower Series	LS, Upper Series	LS, Upper Series	PMS	XPS
Sample:	GR 44	GR 63	GR 27	GM 1496	GM 1496	GR 13	GR 63	GM 1539	GR 27	GM 1496
Mineral:	feldspar	feldspar	feldspar	feldspar	feldspar	nepheline	nepheline	nepheline	nepheline	nepheline
wt %										
SiO_2	66·23	66·49	66·09	65·33	66·74	44·89	44·90	43·47	44·29	44·11
TiO_2	0·02	0·00	0·01	0·03	0·02	0·01	0·00	0·00	0·02	0·00
Al_2O_3	18·40	18·47	18·77	18·54	18·63	31·86	31·79	32·91	32·03	32·12
FeO	0·23	0·16	0·12	0·12	0·19	0·42	0·68	0·29	0·63	0·52
MnO	0·00	0·01	0·00	0·01	0·00	0·02	0·03	0·00	0·01	0·00
MgO	0·01	0·00	0·01	0·00	0·00	0·02	0·00	0·00	0·00	0·00
BaO	0·11	0·15	0·09	0·21	0·13	0·03	0·03	0·00	0·01	0·02
SrO	0·00	0·01	0·00	0·01	0·05	0·00	0·00	0·11	0·00	0·00
CaO	0·04	0·06	0·16	0·18	0·13	0·04	0·00	0·01	0·02	0·01
Na_2O	5·05	5·56	5·98	4·47	5·86	16·15	16·22	16·28	16·24	15·94
K_2O	9·55	8·56	8·14	10·52	8·26	5·56	5·67	6·58	5·84	6·09
Total	99·63	99·46	99·38	99·42	100·01	99·01	99·31	99·66	99·09	98·80
Oxygens p.f.u.	8	8	8	8	8	32	32	32	32	32
Si	3·01	3·01	2·99	2·99	3·00	8·66	8·64	8·40	8·56	8·55
Al	0·98	0·99	1·00	1·00	0·99	7·24	7·21	7·50	7·30	7·34
Ti	0·00	0·00	0·00	0·00	0·00	0·00	0·00	0·00	0·00	0·00
Mg	0·00	0·00	0·00	0·00	0·00	0·01	0·00	0·00	0·00	0·00
Fe^{2+}	0·01	0·01	0·00	0·00	0·01					
Fe^{3+}						0·07	0·11	0·05	0·10	0·08
Mn	0·00	0·00	0·00	0·00	0·00	0·00	0·00	0·00	0·00	0·00
Ba	0·00	0·00	0·00	0·00	0·00	0·00	0·00	0·00	0·00	0·00
Sr	0·00	0·00	0·00	0·00	0·00	0·00	0·00	0·01	0·00	0·00
Ca	0·00	0·00	0·01	0·01	0·01	0·01	0·00	0·00	0·00	0·00
Na	0·44	0·49	0·52	0·40	0·51	6·04	6·05	6·10	6·09	5·99
K	0·55	0·49	0·47	0·61	0·47	1·37	1·39	1·62	1·44	1·51
Total	5·00	4·99	5·00	5·02	4·99	23·39	23·42	23·69	23·50	23·48
Mol %										
An	0·8	0·2	0·3	0·9	0·6					
Ab	52·3	44·5	49·5	38·9	51·6					
Or	46·9	55·3	50·2	60·2	47·8					
Ne						69·8	70·0	72·6	71·1	70·1
Ks						15·8	16·1	19·3	16·8	17·6
Qz						14·4	13·8	8·1	12·1	12·3

Mol % calculations for nepheline as in Wilkinson & Hensel (1994). Ne, nepheline; Ks, kalsilite; Qz, quartz.

well the overall variation in the samples, as the lamellae are volumetrically of minor importance (10–30 vol. %). Except for MnO contents of up to 11·3 wt %, concentrations of minor elements in the reintegrated oxides are low ($Al_2O_3 \leq 0{\cdot}12$ wt %, $MgO \leq 0{\cdot}03$ wt %, $ZnO \leq 0{\cdot}24$ wt %). Late- to post-magmatic hematite associated with biotite has almost a pure hematite end-member composition (Table 3, Fig. 4e).

Minor phases present include short prismatic apatite, zircon, blue sodalite, analcite, calcite and fluorite. Calcite appears to be a primary magmatic or late magmatic interstitial phase and not an alteration product (Fig. 2c). Sodalite can occur as small, interstitial grains, partly associated with cancrinite (Bedford, 1989), or as larger aggregates in almost pure sodalite veins. The chemical characteristics of the minor minerals relevant to this study

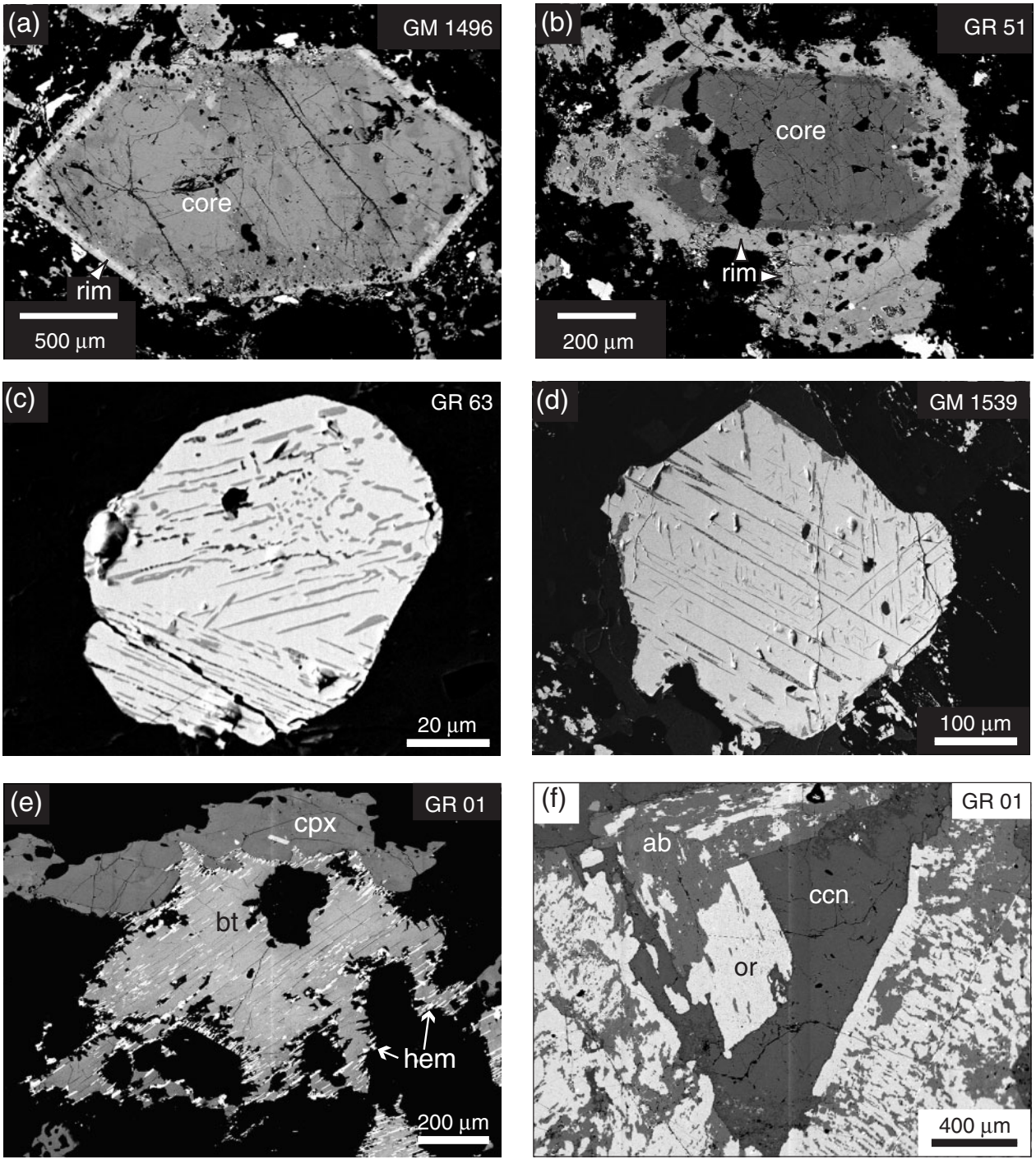

Fig. 4. Back-scattered electron images of minerals in the Grønnedal-Ika syenites. Abbreviations as for Fig. 2, and hem, hematite; ab, albite; or, orthoclase. (a) and (b) Zoning in clinopyroxene phenocrysts from the xenolithic porphyritic syenite; (c) and (d) primary magmatic titanomagnetites showing trellis-type oxy-exsolution into magnetite (light) and ilmenite–pyrophanite–hematite$_{SS}$ (dark lamellae); (e) late- to post-magmatic hematite associated with biotite; (f) perthitic alkali feldspar and cancrinite.

are briefly summarized based on the work of Bedford (1989). Sodalite contains around 8 wt % Cl but only minor amounts (<0·3 wt %) of S. Cancrinite (Fig. 4f), with the ideal structural formula (Sirbescu & Jenkins, 1999) $Na_6Ca_2[Al_6Si_6O_{24}](CO_3)_2 + nH_2O$, also has low (<0·15 wt %) concentrations of S and shows some exchange of Ca for Na. Calcite in the syenites is almost pure $CaCO_3$.

Table 3: Representative electron microprobe analyses of Fe–Ti oxides in Grønnedal-Ika syenites

Unit:	Xenolithic porphyritic syenite			Layered Syenites US			Layered Syenites US			Layered Syenites US			Layered Syenites US
Sample:	GM 1496			GM 1539/3			GM 1539/5			GR 63/5			GM 1539
	mag exs.	ilm exs.	bulk calc.	mag exs.	ilm exs.	bulk calc.	mag exs.	ilm exs.	bulk calc.	mag exs.	ilm exs.	bulk calc.	hem assoc. with bt
wt %													
SiO_2	0·00	0·01	0·00	0·04	0·01	0·03	0·00	0·01	0·00	0·00	0·01	0·00	0·00
TiO_2	0·64	51·64	13·51	0·57	50·03	9·55	0·30	49·38	10·15	0·52	40·93	11·83	0·09
Al_2O_3	0·15	0·04	0·12	0·02	0·01	0·02	0·00	0·00	0·00	0·00	0·01	0·00	0·03
Cr_2O_3	0·02	0·00	0·01	0·00	0·02	0·00	0·01	0·03	0·01	0·00	0·01	0·00	0·00
ZnO	0·12	0·06	0·10	0·05	1·10	0·24	0·02	0·31	0·08	0·04	0·49	0·16	0·02
FeO	92·24	4·42	70·07	91·22	31·23	80·32	90·92	27·45	78·19	92·44	44·58	79·04	89·53
MnO	0·40	43·52	11·29	0·06	15·72	2·90	0·11	20·81	4·26	0·09	10·50	3·00	0·07
MgO	0·00	0·00	0·00	0·03	0·02	0·03	0·03	0·02	0·03	0·03	0·05	0·03	0·01
Total	93·56	99·69	95·11	91·99	98·14	93·11	91·39	98·01	92·72	93·11	96·58	94·08	89·75
Formulae based on 3(2) cations and 4(3) oxygens for mt (ilm)													
Si	0·00	0·00	0·00	0·00	0·00	0·00	0·00	0·00	0·00	0·00	0·00	0·00	0·00
Al	0·01	0·00	0·01	0·00	0·00	0·00	0·00	0·00	0·00	0·00	0·00	0·00	0·00
Ti	0·02	0·98	0·39	0·02	0·97	0·28	0·01	0·95	0·30	0·02	0·79	0·34	0·00
Cr	0·00	0·00	0·00	0·00	0·00	0·00	0·00	0·00	0·00	0·00	0·00	0·00	0·00
Fe^{3+}	1·96	0·04	1·22	1·96	0·07	1·44	1·98	0·09	1·40	1·97	0·41	1·31	2·00
Mg	0·00	0·00	0·00	0·00	0·00	0·00	0·00	0·00	0·00	0·00	0·00	0·00	0·00
Fe^{2+}	1·00	0·05	1·02	1·01	0·60	1·18	1·00	0·49	1·15	1·01	0·55	1·24	0·00
Mn	0·01	0·93	0·37	0·00	0·34	0·10	0·00	0·45	0·14	0·00	0·23	0·10	0·00
Zn	0·00	0·00	0·00	0·00	0·02	0·01	0·00	0·01	0·00	0·00	0·01	0·00	0·00
Total	3·00	2·00	3·00	3·00	2·00	3·00	3·00	2·00	3·00	3·00	2·00	3·00	2·00
Mol %													
Usp	0·02		0·39	0·02		0·28	0·01		0·30	0·02		0·34	
Mag	0·98		0·61	0·98		0·72	0·99		0·70	0·98		0·66	
Ilm		0·05			0·62			0·50			0·56		0·00
Pyr		0·93			0·35			0·46			0·23		0·00
Hem		0·02			0·03			0·05			0·21		1·00
aMag*			0·37			0·52			0·49			0·43	

US, Upper Series; exs., exsolved; calc, calculated; assoc. with bt, associated with biotite.
*aMag was calculated using an ideal mixing model.

Carbonatites

The Grønnedal-Ika carbonatites can be classified as calcite carbonatite and calcite–siderite carbonatite (Woolley & Kempe, 1989) or, on the basis of whole-rock geochemical data with a maximum of 23·1 wt % Fe_2O_3 (Bedford, 1989), as calciocarbonatite and ferruginous calciocarbonatite (Gittins & Harmer, 1997). The carbonatites consist essentially of varying amounts of calcite, siderite and magnetite. They are poor in U–Th–Nb–REE minerals compared with other carbonatites of the world. Magnetite is exclusively secondary after original siderite as a result of decarbonation and oxidation in the vicinity of the dolerite dykes (Bedford, 1989). In places, anhedral to subhedral calcite crystals form almost 100% of the rock (Fig. 2f). Individual calcite crystals are 50–500 μm in diameter and commonly show prominent twinning. Siderite occurs as euhedral rhombs or as minute grains and is commonly rusty-brown because of surface weathering. In the siderite-bearing samples, calcite grains tend to have a cloudy appearance. Minor quantities of apatite,

sphalerite, pyrite, strontianite, monazite, pyrochlore, feldspar and alkali amphibole are also present in some samples (Emeleus, 1964; Bedford, 1989; Bondam, 1992).

GEOCHEMISTRY

Trace elements

Calcite

Chondrite-normalized REE patterns of calcites are shown in Fig. 5a. Three different patterns can be distinguished in the calcites from the carbonatites. One sample—a pure calcite carbonatite (GM 1502)—contains exclusively calcite characterized by a steep REE pattern with high LREE abundances (type A). There is a slight positive Eu anomaly present ($Eu/Eu^* = 1{\cdot}25$) and the degree of LREE enrichment relative to the HREE expressed as La_{CN}/Yb_{CN} is ~69. The overall REE enrichment of this sample is within the lower range of whole-rock analyses from the Grønnedal carbonatite and typical of carbonatites in general (Woolley & Kempe, 1989). Two distinctly different types of REE patterns occur in calcites from sample GM 1498, where type A patterns are absent. The sample is a calcite–siderite carbonatite in which siderite is characterized by brown oxidation rims. Both REE patterns show a strong depletion in LREE relative to the type A pattern (Fig. 5a). The main characteristic of the type B REE pattern is a convex-upward shape. In contrast, type C calcite has about one order of magnitude lower normalized LREE and MREE abundances and exhibits an almost continuous increase from very low LREE abundances towards the HREE. There are no textural differences between types B and C. Interstitial calcite from two syenitic samples (Layered Syenites, samples GR 44 and GR 63) shows LREE-enriched patterns similar to type A, but with slight negative Eu anomalies ($Eu/Eu^* = 0{\cdot}66$) and a flatter slope ($La_{CN}/Yb_{CN} = 10{\cdot}5–26{\cdot}3$). In a similar fashion, the REE pattern of the XPS whole-rock matrix is flatter than that of the whole-rock carbonatites (Fig. 5a). In addition to the REE, Sr, Ba, Pb, Y and Ga also occur in significant amounts in the calcites, whereas all calcites have very low concentrations of the HFSE (e.g. Nb, Ta, Zr, Hf), mostly below the detection limits (Table 4). Type A calcite (GM 1502) is characterized by a relative enrichment of Ba, Sr, Eu and Ga compared with the calcites from the syenites (Fig. 6a). Type B and C calcites show marked enrichments in Pb and Sr compared with the neighboring elements. These features and the low REE contents of type B and C calcite are not entirely clear. They are consistent with postmagmatic loss of these elements by fluid-controlled recrystallization and remobilization of carbonate phases (Bau, 1991; Bau & Möller, 1992), for which brown rims around siderite might be an indication, or they could be related to the contemporaneous siderite crystallization itself.

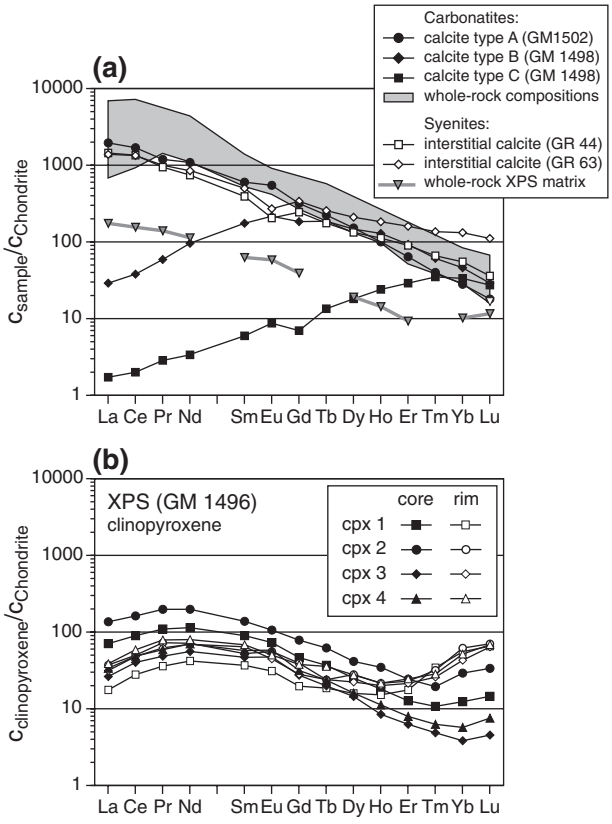

Fig. 5. Chondrite-normalized REE patterns, normalized relative to the chondritic values of Boynton (1984). (a) calcite from carbonatites and syenites; comparative whole-rock data from Bedford (1989) and Goodenough (1997); (b) clinopyroxenes from the xenolithic porphyritic syenite (sample GM 1496).

Clinopyroxene

A detailed study of the REE and trace-element abundances in clinopyroxene and amphibole in the Grønnedal-Ika syenites has been made by Marks *et al.* (2004*a*). In this study, we concentrate on data from clinopyroxene phenocrysts in the XPS to evaluate whether features of the trace-element chemistry indicative of silicate–carbonate liquid immiscibility can be detected. Typical trace-element concentrations in clinopyroxene cores and rims are summarized in Table 4. Chondrite-normalized REE patterns (Fig. 5b) indicate distinct differences between core and rim compositions. The core patterns are characterized by a smooth increase in normalized abundances from La to Nd and a smooth decrease from Nd to Tm or Yb, with a slight increase towards Lu. La_{CN}/Yb_{CN} ratios in the cores range from 4·7 to 6·9 and Eu anomalies are slightly positive, with values between 1·02 and 1·37. In the Na-rich rims, REE

Table 4: Average trace-element compositions of clinopyroxene and calcite in Grønnedal-Ika rocks determined by laser ablation ICP–MS

Rock type:	XPS	XPS	XPS	XPS	Carbonatite	Carbonatite	Carbonatite	Syenite	Syenite
Sample:	GM 1496	GM 1496	GM 1496	GM 1496	GM 1502	GM 1498	GM 1498	GR 44	GR 63
n:	9	1	3	1	6	2	5	7	5
Mineral:	cpx 1 core	cpx 1 rim	cpx 4 core	cpx 4 rim	calcite type A	calcite type B	calcite type C	interstitial calcite	interstitial calcite
ppm									
Cs	0·27	—	—	—	—	—	—	—	—
Rb	2·98	0·44	9·89	0·45	—	—	—	—	—
Ba	1·34	—	2·21	1·06	5486	76·2	12·0	54·1	106
Th	0·08	—	0·11	0·27	0·34	—	—	0·12	0·15
U	0·04	—	0·04	—	—	—	—	—	0·01
Nb	1·93	1·79	2·97	2·47	0·59	—	—	—	—
Ta	0·23	0·11	0·38	0·47	—	—	—	—	—
La	21·9	5·46	10·5	12·0	606	8·89	0·53	447	429
Ce	72·5	22·5	39·1	47·5	1367	30·5	1·61	1091	1081
Pb	0·22	0·25	0·77	0·47	24·3	25·5	51·9	12·8	24·2
Pr	13·4	4·38	7·20	9·63	145	7·21	0·35	115	122
Sr	392	282	607	414	15115	6110	5620	8753	6166
Nd	68·5	25·2	42·1	47·9	652	57·7	2·02	446	508
Zr	381	5529	237	5557	0·35	—	—	0·31	—
Hf	10·3	94·1	7·51	122	—	—	—	—	—
Sm	17·5	7·18	11·2	13·3	117	34·1	1·16	76·5	97·4
Eu	5·4	2·28	4·28	3·69	40·2	15·9	0·64	15·1	19·9
Ti*	2098	1918	2098	1918	n.a.	n.a.	n.a.	n.a.	n.a.
Sn	2·53	34·6	1·86	37·0	0·76	0·67	0·47	—	—
Gd	12·0	5·10	8·16	9·80	82·1	47·5	1·81	63·1	87·9
Tb	1·75	0·88	1·12	1·69	10·6	8·81	0·64	8·33	12·2
Dy	8·08	5·11	5·15	8·90	48·8	47·3	5·83	43·0	67·5
Li	10·9	—	26·2	2·96	—	—	—	—	—
Y	27·8	19·2	16·8	31·7	160	184	35·8	191	297
Ho	1·30	1·09	0·81	1·55	7·20	9·24	1·73	8·03	13·2
Er	2·67	3·70	1·67	5·15	13·5	19·6	6·08	18·9	33·7
Tm	0·35	1·11	0·20	0·92	1·31	1·99	1·13	2·15	4·40
Yb	2·59	11·6	1·19	10·8	5·92	9·71	7·00	11·5	27·7
Lu	0·47	2·11	0·24	2·21	0·58	0·93	0·88	1·16	3·56
Sc	6·51	3·19	5·29	—	1·51	—	1·80	—	—
V	2·16	6·38	82·2	12·1	—	—	—	—	—
Co	19·8	7·38	23·4	9·91	1·85	1·46	1·57	—	1·08
Zn	113	403	105	372	7·24	20·0	21·7	1·87	4·83
Ga	12·3	26·3	18·1	14·8	50·9	1·07	—	2·83	5·44
La_{CN}/Yb_{CN}	5·71	0·32	5·91	0·75	68·98	0·62	0·05	26·29	10·46
Eu/Eu*	1·13	1·15	1·37	0·99	1·25	1·21	1·35	0·66	0·66
Zr/Hf	36·9 ± 1·6	58·8	31·5 ± 2·2	45·7					
Y/Ho	21·4 ± 1·3	17·6	20·7 ± 3·4	20·5	22·3 ± 1·1	19·9 ± 1·5	20·8 ± 1·0	23·8 ± 1·9	22·5 ± 0·8

n, number of spot analyses; Eu/Eu*, $Eu_{CN}/(Sm_{CN} \times Gd_{CN})^{0.5}$; —, not detected; n.a., not analysed; *determined by microprobe. Zr/Hf and Y/Ho ratios are given as the average and the 1σ standard deviation of the individual spot analyses.

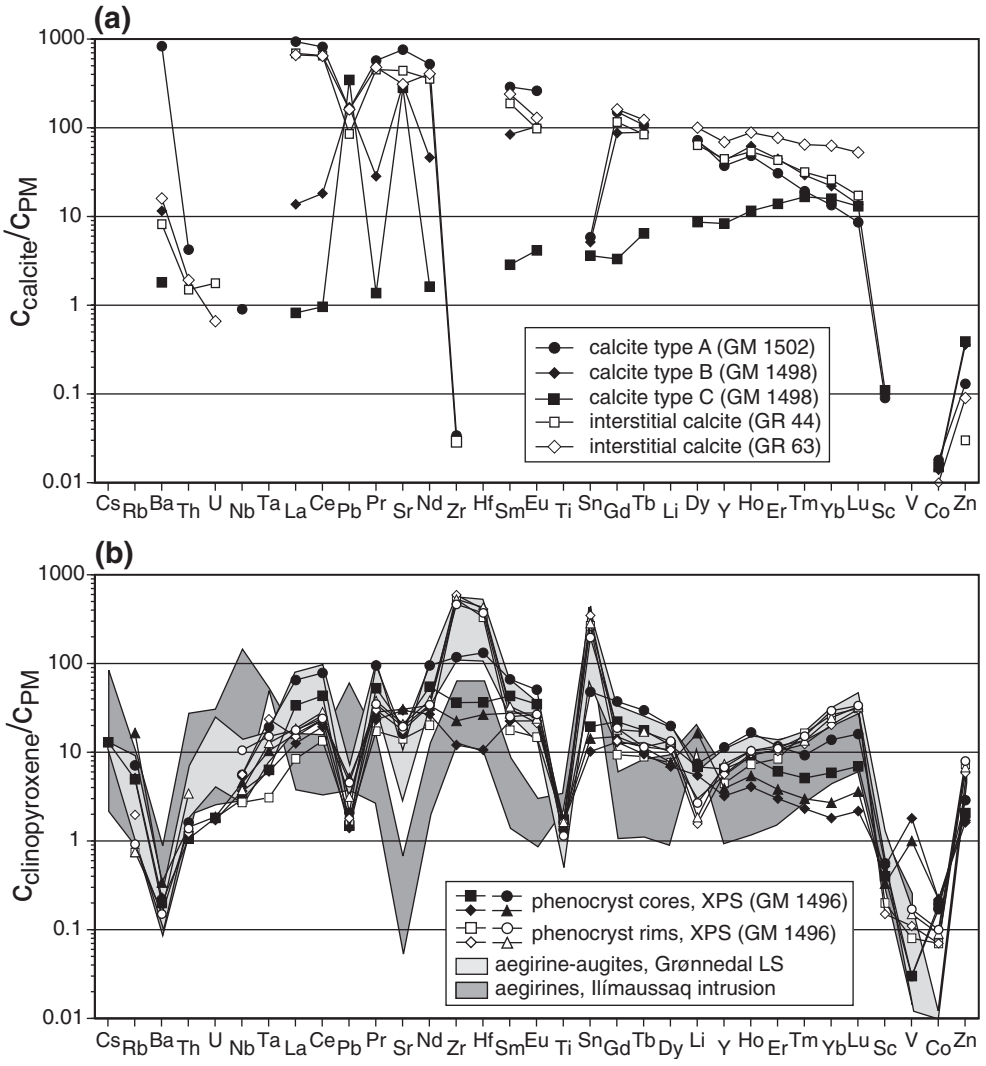

Fig. 6. Multi-element trace element diagram for calcite and clinopyroxenes from the Grønnedal-Ika rocks, normalized relative to primitive mantle values (McDonough & Sun, 1995). (a) Calcite from carbonatites and syenites; (b) clinopyroxenes from the xenolithic porphyritic syenite; shaded fields show comparative data from Marks *et al.* (2004*a*).

patterns are sinusoidal with generally lower LREE and higher HREE abundances than in the cores (Fig. 5b). La_{CN}/Yb_{CN} ratios range between 0·32 and 0·75. Eu anomalies in the rims are not significantly different from those in the cores and vary from 0·99 to 1·24.

Trace-element concentrations of XPS clinopyroxene cores and rims normalized to primitive mantle values (McDonough & Sun, 1995) are shown in Fig. 6b. A principal feature of all the patterns are strong negative Ba, Pb and Ti spikes and depletions in Sc, V and Co. Negative Sr spikes are present in all patterns except for two phenocryst cores. These two cores are also characterized by the lowest Zr and Hf values. All rim compositions have strong positive Zr, Hf and Sn, but negative Li anomalies. In comparison with the core compositions, rims are also enriched in Zn, but depleted in Rb, Co and Sc. All rim patterns are very similar to those of aegirine–augites from the LS, both in enrichment level and shape (Fig. 6b). Aegirines from another silica-undersaturated syenitic complex of the Gardar Province, Ilímaussaq (Marks *et al.*, 2004*a*) have much lower absolute trace-element concentrations, but the shape of their patterns has a striking similarity to that of the phenocryst rims, except for Li and Pb.

Ratios of isovalent trace elements with a similar geochemical behavior (Bau, 1996) were investigated in order to identify characteristic differences between the growth of clinopyroxene cores and rims (Fig. 7). Zr/Hf ratios in the cores vary between 31·5 and 42·1, and scatter around the primitive mantle value of 37·1 (McDonough & Sun,

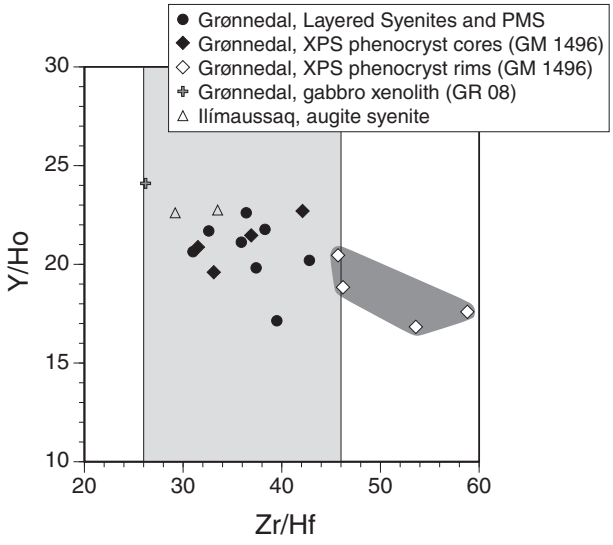

Fig. 7. Y/Ho vs Zr/Hf diagram for clinopyroxenes in syenites from the Grønnedal-Ika and Ilímaussaq intrusions [Ilímaussaq data from Marks *et al.*, (2004*a*)]. The light grey shaded field defines the Zr/Hf ratios of common igneous rocks crystallizing from silica melt systems (Bau, 1996). The dark grey shaded field highlights the XPS clinopyroxene rim compositions.

1995). In the rims, however, Zr/Hf ratios are higher than in the cores, with values ranging from 45·7 to 58·8. In contrast, Y/Ho ratios in individual phenocrysts are slightly higher in the cores (Y/Ho = 19·6–22·7) compared with the rims (Y/Ho = 16·8–20·5). Nb/Ta ratios scatter widely (Nb/Ta = 4·2–16·3) and there is no consistent relation between core and rim compositions.

Carbon and oxygen isotope analyses

Goodenough (1997), Pearce *et al.* (1997), Coulson *et al.* (2003) and Taubald *et al.* (2004) have reported C and O isotopic data from Grønnedal-Ika, but data on silicates from the syenites were lacking so far. Recent oxygen isotope studies have shown that individual coarse-grained minerals are less sensitive to low-T alteration than whole-rock samples (e.g. Vroon *et al.*, 2001). Extensive studies of mineral separates from ocean island basalts (Eiler *et al.*, 1997) and oceanic-arc lavas (Eiler *et al.*, 2000*a*) demonstrated that analyses of mineral separates consistently span a narrower range than comparable whole-rock data. At Grønnedal-Ika, whole-rock oxygen and carbon isotope data were used as an argument against liquid immiscibility between syenites and carbonatites because of their distinct differences in $\delta^{18}O_{V\text{-}SMOW}$ and $\delta^{13}C_{PDB}$ (Pearce *et al.*, 1997). To evaluate this argument in the view of mineral data, the oxygen isotope compositions of fresh magmatic clinopyroxene and amphibole in the syenites were measured, augmented by C and O isotopic data of microdrilled calcite (Table 5).

Table 5: O and C isotope composition of minerals from the Grønnedal-Ika intrusion

Sample	Sample material	$\delta^{18}O_{V\text{-}SMOW}$ (‰)	$\delta^{13}C_{PDB}$ (‰)
Layered Syenites			
Lower Series			
GR 01	cpx	4·8/4·9	
GR 36	cpx	4·6	
GR 10	cpx	4·8	
GR 13	cpx	4·9/4·8	
GM 1554	cpx	4·4	
Upper Series			
GR 15	cpx	4·8	
GM 1526	cpx	4·7	
GR 44	cpx	4·3	
GM 1559	cpx	4·2	
GM 1531	amph	4·6/4·7	
GR 63	cpx	4·8	
GM 1539	cpx	4·6	
PMS and XPS			
GR 18 — PMS	cpx	4·8	
GR 27 — PMS	cpx	4·3	
GR 51 — XPS	cpx	4·5	
GM 1496 — XPS	cpx	4·2	
Gabbroic xenolith			
GR 08	cpx	5·2/5·1	
Carbonatites			
GR 46	calcite	7·9	−4·7
GR 70	calcite	8·6/8·6	−4·4/−4·2
GR 73	calcite	8·4/8·2	−4·3/−4·4
GR 74	calcite	7·9	−4·6
GM 1498	calcite	8·0	−3·9
GM 1502A	calcite	7·9	−3·9
GM 1502B	calcite	7·9	−4·0

PMS, porphyritic microsyenite; XPS, xenolithic porphyritic syenite.

The oxygen isotopic composition of clinopyroxene from the syenites varies from 4·2 to 4·9‰ and that of amphibole ($\delta^{18}O$ = 4·7‰) is within this range. The average $\delta^{18}O$ value of clinopyroxene from the layered syenites is 4·6‰ ± 0·2‰ (1σ). There is no significant isotopic compositional difference between the layered syenites and the late syenites. It was not possible to analyze core and rim compositions in the clinopyroxenes from the XPS separately, but, from petrographic observations, the proportion of rim composition in the clinopyroxene population should be relatively small compared with the core composition. $\delta^{18}O$ values of clinopyroxene from the XPS are in the lower range of

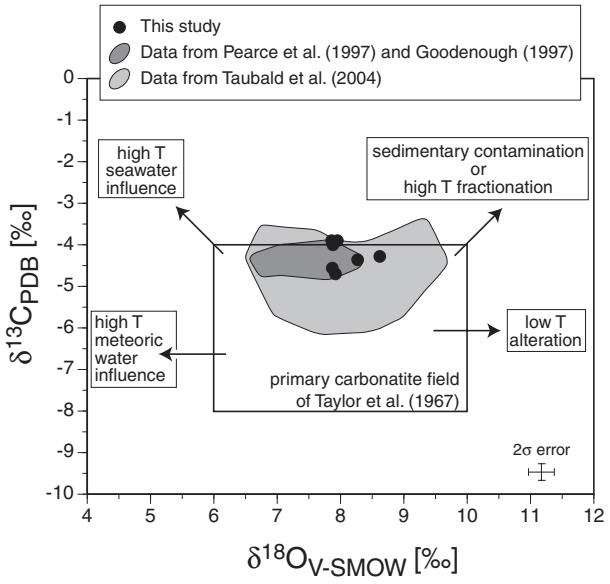

Fig. 8. Carbon and oxygen isotope composition of calcite from Grønnedal-Ika carbonatites, together with the field of primary, unaltered carbonatites of Taylor *et al.* (1967). Arrows indicate schematically the main processes responsible for changes in the C–O isotopic compositions (after Deines, 1989 and Demény *et al.*, 1998). Comparative data are whole rocks and separated carbonate phases from Grønnedal-Ika carbonatites (dark grey field: Goodenough, 1997; Pearce *et al.*, 1997; light grey field: Taubald *et al.*, 2004).

the entire dataset. Clinopyroxene from a gabbroic xenolith (sample GR 08) is slightly, but significantly, higher in $\delta^{18}O$ than from the syenites, with $\delta^{18}O = 5{\cdot}1‰$.

In the studied suite of samples, the oxygen isotope composition of calcite ranges from 7·8 to 8·6‰ $\delta^{18}O$ and carbon isotope composition varies between −3·9 and −4·7‰ $\delta^{13}C$. Our data overlap with the data from the literature. They are shown in Fig. 8, together with the field of primary, mantle-derived carbonatites as proposed by Taylor *et al.* (1967). The C and O isotopic compositions of the Grønnedal-Ika carbonates are within the upper half of the primary carbonatite field of Taylor *et al.* (1967).

Nd isotope analyses

Nd isotopic analyses of mineral separates and whole-rock samples are presented in Table 6. $\varepsilon_{Nd}(T)$ values were calculated for T = 1300 Ma based on the Rb–Sr isochron age of the complex (Blaxland *et al.*, 1978). They range from +1·8 to +2·8 for the syenites and from +2·4 to +2·8 for the carbonatites. The average $\varepsilon_{Nd}(T)$ of the carbonatites (2·59 ± 0·20) is slightly higher, but not significantly different from the average of the syenites (2·36 ± 0·40). Thus, the Nd isotopic composition of the Grønnedal-Ika complex appears to be relatively homogeneous. However, $\varepsilon_{Nd}(T)$ is slightly lower compared with whole-rock syenite data from Grønnedal-Ika (ε_{Nd} = 3·2–3·9; Goodenough, 1997) and a value for the Gardar mantle source ($\varepsilon_{Nd} > 4$) defined by Andersen (1997). Plotted in a Sm–Nd isochron diagram (Fig. 9), all analyses of the mafic minerals and the carbonatites scatter closely around the 1300 Ma reference line. Clinopyroxene from a gabbroic xenolith (sample GR 08) yielded a distinctly lower $\varepsilon_{Nd}(T)$ value than those typical for the syenites [$\varepsilon_{Nd}(T) = -1{\cdot}7$]. A whole-rock sample of relatively unaltered basement gneiss has $\varepsilon_{Nd}(T) = -13{\cdot}3$.

CALCULATION OF PHYSICO-CHEMICAL PARAMETERS

Temperature, silica activity and oxygen fugacity in the nepheline syenites

The quantification of intensive crystallization parameters can be used to distinguish separate phases in the evolution of the complex or individual units. Furthermore, the determination of equilibration temperatures is important for obtaining accurate estimates of the oxygen isotope composition of the melt from the mineral data, because mineral–melt isotopic exchange is temperature dependent. The quantification of silica activities and oxygen fugacities is relevant for comparison with other Gardar complexes to evaluate the possible influence of these parameters on the origin of the carbonatite.

Equilibria among Ne, Ab and Jd components in nepheline, alkali feldspar and clinopyroxene solid solutions, respectively, provide means to estimate temperatures and silica activities in nepheline syenites (Markl *et al.*, 2001). These equilibria are believed to reflect the conditions during formation of the last mineral in a specific assemblage (Markl *et al.*, 2001). In the absence of a reliable pressure estimate, 1 kbar was used for all calculations. This value is an estimate from the Ilímaussaq intrusion further south in the Gardar Province, based on fluid inclusion studies (Konnerup-Madsen & Rose-Hansen, 1984). For the nepheline syenites of Grønnedal-Ika, the following three equilibria are relevant:

$$\text{albite (in alkali feldspar)} = \text{jadeite (in cpx)} + SiO_2 \quad (1)$$

$$\text{albite (in alkali feldspar)} = \text{nepheline} + 2SiO_2 \quad (2)$$

$$\text{nepheline} + SiO_2 = \text{jadeite (in cpx)}. \quad (3)$$

Following the approach of Markl *et al.* (2001), we assume equilibration of the magmatic mineral assemblage is achieved as long as melt remained in contact with the minerals and in the absence of growth zonation (feldspars and nephelines). Zoned clinopyroxene crystals record various stages of crystallization, and

Table 6: Mineral separate and whole-rock Nd isotope analyses from Grønnedal-Ika

Sample	Type	Sm (ppm)	Nd (ppm)	$^{147}Sm/^{144}Nd$	$^{143}Nd/^{144}Nd$	$^{143}Nd/^{144}Nd(T)$	$\varepsilon_{Nd}(T)$	$\varepsilon_{Nd}(0)$	T_{DM}*	T_{CHUR}
Layered Syenites										
Lower Series										
GR 01	cpx	17·42	81·65	0·1290	0·512205 ± 10	0·511103	2·8	−8·4	1·60	0·97
GR 13	cpx	27·56	139·29	0·1196	0·512120 ± 10	0·511099	2·7	−10·1	1·58	1·02
Upper Series										
GR 15	cpx	27·21	133·23	0·1235	0·512120 ± 07	0·511066	2·1	−10·1	1·64	1·08
GR 44	cpx	43·37	243·51	0·1077	0·511971 ± 10	0·511052	1·8	−13·0	1·61	1·14
GR 63	cpx	35·85	179·91	0·1205	0·512081 ± 10	0·511052	1·8	−10·9	1·65	1·11
GM 1531	amph	12·06	71·65	0·1018	0·511969 ± 09	0·511100	2·8	−13·1	1·53	1·07
GM 1559	cpx	32·56	160·78	0·1224	0·512115 ± 10	0·511070	2·2	−10·2	1·63	1·07
PMS and XPS										
GR 27 — PMS	cpx	33·79	170·24	0·1200	0·512115 ± 10	0·511091	2·6	−10·2	1·59	1·04
GM 1496 — XPS	cpx	15·72	69·67	0·1364	0·512243 ± 10	0·511078	2·3	−7·7	1·67	1·00
Gabbroic xenolith										
GR 08	cpx	16·66	63·05	0·1598	0·512236 ± 09	0·510872	−1·7	−7·8	2·34	1·66
Carbonatites										
GR 46	whole rock	243·83	1587·0	0·0929	0·511891 ± 10	0·511098	2·7	−14·6	1·52	1·10
GR 70	whole rock	54·37	374·06	0·0879	0·511852 ± 10	0·511102	2·8	−15·3	1·51	1·10
GR 73	whole rock	235·97	1260·3	0·1132	0·512049 ± 09	0·511083	2·4	−11·5	1·58	1·07
GR 74	whole rock	344·58	1915·4	0·1088	0·512010 ± 09	0·511081	2·4	−12·3	1·57	1·09
Basement gneiss										
GR 78	whole-rock	4·492	20·74	0·1309	0·511399 ± 11	0·510281	−13·3	−24·2	3·01	2·85

*T_{DM} calculated with $(^{147}Sm/^{144}Nd)_{DM} = 0·219$ and $(^{143}Nd/^{144}Nd)_{DM} = 0·513151$.
PMS, porphyritic microsyenite; XPS, xenolithic porphyritic syenite. Calculations of $^{143}Nd/^{144}Nd(T)$ and $\varepsilon_{Nd}(T)$ for $T = 1·30$ Ga (Blaxland *et al.*, 1978).

the increase in Na^+ and Fe^{3+} in clinopyroxene rims and along cracks may reflect oxidation by residual melt or fluid phases (Marks *et al.*, 2003). Therefore, estimates of magmatic T and $aSiO_2$ conditions were made using clinopyroxene compositions that presumably reflect early crystallization, i.e. the most diopside-rich compositions of the matrix clinopyroxenes. Activities of jadeite in clinopyroxene (a_{Jd}) were calculated after Holland (1990) at temperatures of 800, 900 and 1000°C. For feldspars, the complete range of compositions measured was used to determine the activity of albite (a_{Ab}) after Fuhrman & Lindsley (1988), again at 800, 900 and 1000°C. Nepheline activities (a_{Neph}) were calculated using a mixing-on-sites model and do not show a large variation, either between or within samples. Therefore, an average a_{Neph} for each sample was used. Input parameters and results are summarized in Table 7. Calculations using minimum and maximum values for a_{Jd} and a_{Ab} resulted in four positions of the same invariant point that define parallelogram-shaped fields in T–$aSiO_2$ space (Fig. 10). These fields are considered to represent the equilibration conditions of the assemblage.

For the LS and the PMS, equilibrium conditions vary from 680 to 850°C and $aSiO_2$ values of 0·28–0·41 (Table 7). Temperatures agree well with those obtained by nepheline geothermometry after Hamilton (1961), which yields temperatures between 700 and 850°C. Only a few nepheline analyses poor in SiO_2 indicate temperatures as low as 500°C, which suggests prolonged re-equilibration (Powell, 1978). Calculations with a higher crystallization pressure of 2 kbar yield slightly higher temperatures and silica activities, but this does not affect the general conclusions of this study. For the XPS, calculations were performed with clinopyroxene compositions from phenocryst cores, phenocryst rims and matrix grains, as it is not clear from petrographic observations which clinopyroxene equilibrated with the nepheline and feldspar. Calculations with the most

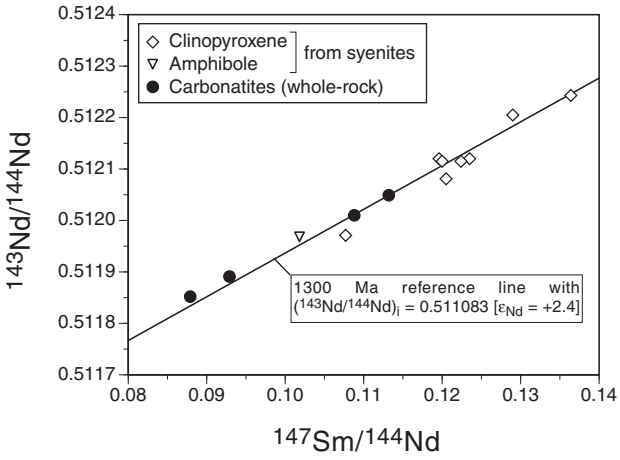

Fig. 9. Sm–Nd isochron diagram for clinopyroxene and amphibole mineral separates from syenites and whole-rock carbonatites from Grønnedal-Ika. The 1300 Ma reference line is based on the Rb–Sr age of 1299 ± 17 Ma (Blaxland *et al.*, 1978). Errors (±0·5% for $^{147}Sm/^{144}Nd$ and ±0·002% for $^{143}Nd/^{144}Nd$) are not larger than the symbols.

Mg-rich matrix cpx compositions indicate temperatures of 710–775°C and silica activities of 0·28–0·36. Equilibria with Mg-rich rim compositions yield similar but slightly elevated values of $a SiO_2$ (0·32–0·43) and temperatures of 785–910°C. For both matrix and phenocryst rim compositions, calculated values of T and $a SiO_2$ overlap with the intensive parameters determined for the Layered Syenites. However, equilibria based on typical phenocryst core compositions (a_{Jd} = 0·08–0·12) yield temperatures of <550°C at silica activities <0·25. It is very unlikely that the cores grew at such low temperatures, and most probably the clinopyroxene core compositions were not in equilibrium with nepheline and alkali feldspar during growth. Thus, we believe that the clinopyroxene phenocryst cores of the XPS crystallized during a distinct earlier event in the magmatic history, possibly as the only crystallizing phase or at higher *P*.

The abundant occurrence of cancrinite (Fig. 4f) suggests a considerable build-up in CO_2 in the late stages of the solidification of the magma, as cancrinite crystallization temperatures, derived from fluid inclusion data, range from 450 to 650°C at 1·1–1·5 kbar (Sobolev *et al.*, 1974). This enrichment of CO_2 might be linked to the forcible emplacement of the carbonatite into the nepheline–syenites.

Oxygen fugacities in the nepheline syenites were estimated from the compositions of reintegrated titanomagnetites, and independent temperature determinations from Ne–Ab–Jd equilibria. In Fig. 11, theoretical oxygen buffer curves (FMQ, HM) are plotted together with their displaced positions appropriate to the activities determined from mineral analyses in this study (FMQ*, HM*, FsMQ*). FMQ* marks the minimum oxygen fugacity in the nepheline syenites, as this is the position of the buffer curve recalculated with mineral compositions typical for the syenites ($a SiO_2$ = 0·37, a_{Mag} = 0·43) if olivine with a_{Fa} = 1 were present. At high temperatures, Fe–Ti oxides equilibrate readily with a fluid phase because of their fast reaction kinetics in hydrothermal experiments (Buddington & Lindsley, 1964), and it can be inferred that this is true for melts as well. Then, for a given temperature and magnetite–ulvöspinel$_{SS}$ composition, the fO_2 of the fluid–melt can be read from the fO_2–T graph (Fig. 11). Because this fluid–melt phase, in turn, determines the fO_2 of the rock (Buddington & Lindsley, 1964), we can estimate the oxygen fugacities of the nepheline syenitic melts at their equilibration temperatures of 710–910°C with the typical oxide composition $Mag_{60–70}Usp_{30–20}$. The latter are represented as projections of tie-lines connecting coexisting magnetite–ulvöspinel$_{SS}$ and hematite–ilmenite$_{SS}$ pairs after Buddington & Lindsley (1964) and they define a dark grey shaded field in Fig. 11. At temperatures appropriate for the syenites (700–910°C) fO_2 falls between +2 and +5 log units above the FMQ buffer (cross-hatched pattern in Fig. 11). This result agrees well with the position of the FsMQ* (ferrosilite–magnetite–quartz) buffer at very low a_{Fs} values (≤0·01) that corresponds to the virtually absent ferrosilite component in the aegirine–augites. The occurrence of presumably late- to post-magmatic hematite indicates that oxygen fugacities increased to values >1 log unit above the HM buffer during the later stages of magmatic evolution (light grey arrow).

Stable isotope composition of the Grønnedal-Ika magmas

Oxygen isotopes in nepheline syenites

Oxygen isotope data for mineral separates from Grønnedal-Ika and other Gardar igneous rocks (Halama *et al.*, 2003; Marks *et al.*, 2003) are plotted in Fig. 12a versus the respective $\varepsilon_{Nd}(T)$ values. Compared with the Eriksfjord Formation basalts, samples from Grønnedal-Ika syenites have slightly lower $\delta^{18}O$ values at slightly higher values of $\varepsilon_{Nd}(T)$. Clinopyroxene from the gabbroic xenolith overlaps with the EF basalt samples. In contrast, most minerals from the silica-oversaturated rocks from the Puklen intrusion tend towards lower $\delta^{18}O$ values and strongly negative $\varepsilon_{Nd}(T)$ values, which were interpreted to reflect the influence of open-system late-stage magmatic processes and assimilation of crustal material (Marks *et al.*, 2003). These factors do not seem to have affected the Grønnedal-Ika rocks. However, not only the oxygen isotopic composition of the melt, but also temperature and chemical composition of the minerals influence $\delta^{18}O_{mineral}$ values (Zheng, 1993*a*,

Table 7: Activities used in calculations for jadeite–albite–nepheline equilibria and resulting temperatures and silica activities of syenitic rocks from Grønnedal-Ika

Sample	Comment	a_{Jd}		a_{Ab}		a_{Neph}	Calculated temperatures (°C)	Calculated silica activities
		min.	max.	min.	max.	average		
Layered Syenites								
GR 44		0·038	0·050	0·66	0·79	0·73	680—810	0·28—0·38
GR 63		0·035	0·042	0·70	0·80	0·74	750—850	0·33—0·41
GM 1539		0·042	0·046	0·67	0·81	0·74	710—780	0·30—0·37
GM 1559		0·036	0·047	0·66	0·76	0·74	700—830	0·30—0·38
PMS and XPS								
PMS — GR 27		0·042	0·051	0·68	0·79	0·74	680—780	0·29—0·36
XPS — GM 1496	equilibria with phenocryst cpx rims	0·031	0·035	0·59	0·79	0·74	785—910	0·32—0·43
XPS — GM 1496:	equilibria with matrix cpx	0·042	0·044	0·59	0·79	0·74	710—775	0·28—0·36

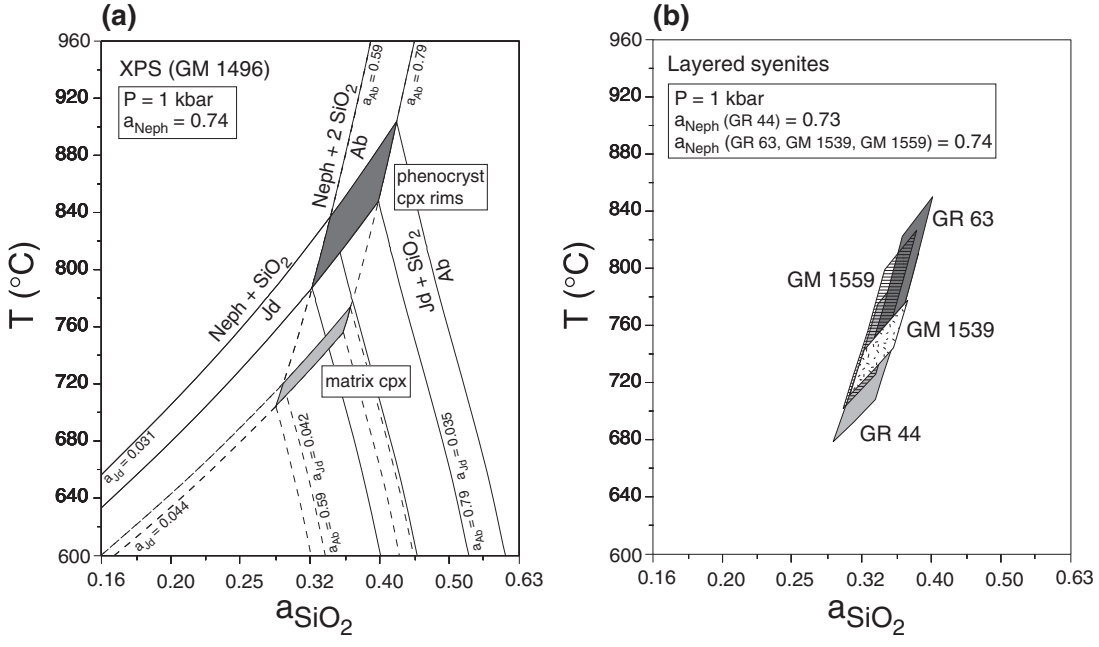

Fig. 10. Temperature vs silica activity diagrams showing equilibria between Ab, Ne and Jd for the syenitic rocks of Grønnedal-Ika. All calculations were performed using an extension of the GEO-CALC software (Berman *et al.*, 1987; Lieberman & Petrakakis, 1991). Note that the *x*-axis values are based on a $\log_{10}$ scale. (a) Ab–Ne–Jd in matrix clinopyroxene (light grey field) and Ab–Ne–Jd in clinopyroxene phenocryst rims (dark grey field) equilibria, calculated for constant P (1 kbar) and nepheline activity ($a_{Neph} = 0{\cdot}74$) and minimum and maximum Ab and Jd activities determined in the respective minerals; thus, four different positions of the same invariant point are obtained, which define the parallelogram-shaped fields; (b) fields defined by the four invariant points of the Ab–Ne–Jd equilibria as described in (a) for four samples from the Layered Syenites.

1993*b*). Therefore, it is useful to calculate $\delta^{18}O_{melt}$ from the mineral data. The calculation of the oxygen isotopic composition of the original melts from mineral data is relatively straightforward for basaltic rocks (Kalamarides, 1986), but less so for the Grønnedal samples because of lower equilibration temperatures and the formation of diopside–aegirine solid solutions. We therefore used a different approach, which is briefly described below.

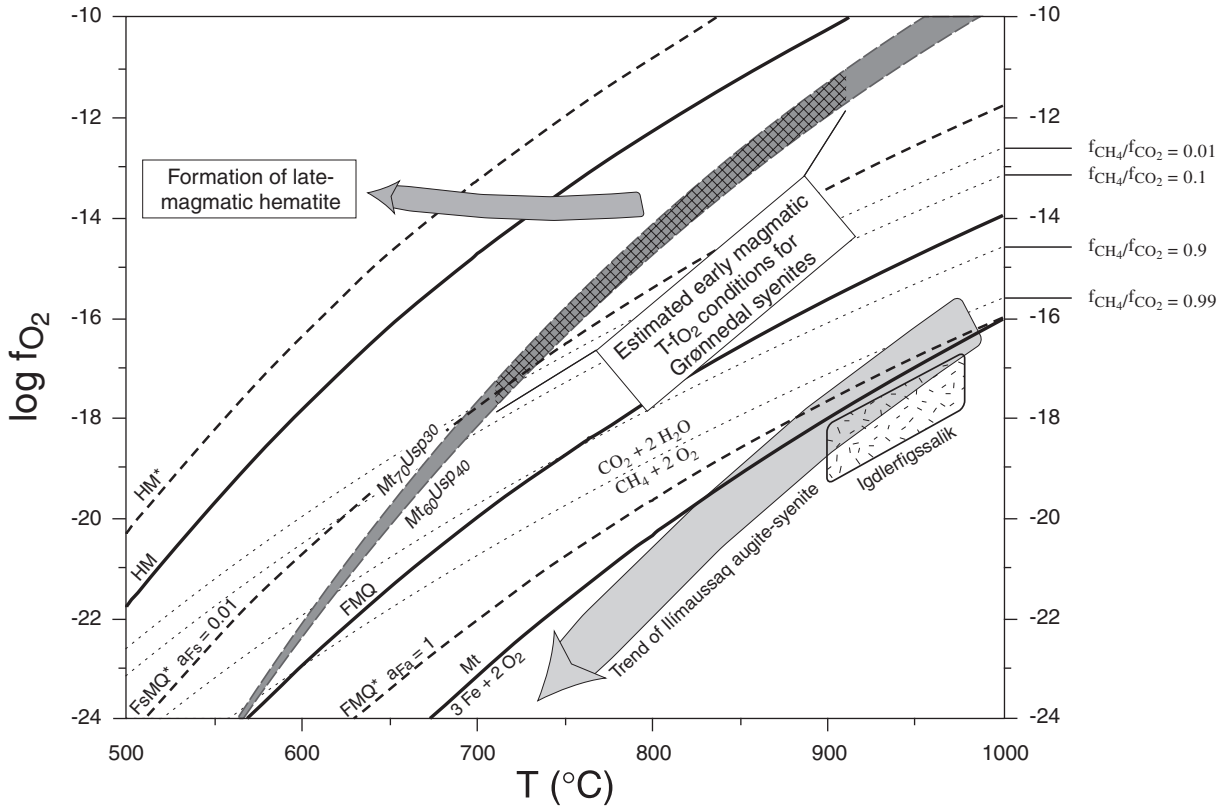

Fig. 11. fO_2–T diagram with estimated formation conditions of early- and late-magmatic Fe–Ti oxides in the Grønnedal-Ika syenites. FMQ and HM are the fayalite–magnetite–quartz and the hematite–magnetite buffer. FMQ* is the displaced FMQ buffer recalculated with mineral compositions typical values of the syenites ($a_{SiO_2} = 0{\cdot}37$, $a_{Mag} = 0{\cdot}43$). The same activities were used to calculate the position of the displaced buffer reaction 3ferrosilite + O_2 = 2magnetite + $6SiO_2$ (FsMQ*). HM* shows the displaced position of the HM buffer representative for the syenitic samples with $a_{Hem} = 0{\cdot}98$ and $a_{Mag} = 0{\cdot}43$. These calculations were performed using an extension of the GEO-CALC software (Berman *et al.*, 1987; Lieberman & Petrakakis, 1991). Tie-line projections connecting conjugate magnetite–ulvöspinel$_{SS}$ and hematite–ilmenite$_{SS}$ pairs after Buddington & Lindsley (1964) are shown for magnetite compositions typical of the Grønnedal-Ika samples. They define the dark grey field (see text for discussion). Stippled curves indicate the position of the equilibrium $CH_4 + 2O_2 = 2H_2O + CO_2$ with C:H = 1:2 and variable fCH_4/fCO_2 ratios (calculations assume ideal gas behavior, P_{total} = 1 kbar and C:H = 1:2; thermodynamic data from Robie & Hemingway, 1995). The grey arrow shows a possible evolution path of the Grønnedal-Ika syenitic magmas. The trend of the augite syenite unit from the Ilímaussaq intrusion is from Markl *et al.* (2001); the field for the Igdlerfigssalik syenites (confetti pattern) represents conditions for cumulus crystallization after Powell (1978).

Based on the nepheline–albite–jadeite equilibria, we assume that the equilibration temperature (T_{eq}) for all nepheline syenitic samples is ~800°C. In a first step, the mineral–water oxygen isotope fractionation was calculated after Zheng (1993*a*, 1993*b*) at T_{eq} using a typical aegirine–augite composition of $Di_{30}Hd_{40}Aeg_{30}$. Secondly, the rock–water oxygen isotope fractionation of a typical nepheline syenite at T_{eq} was determined after Zhao & Zheng (2003). The two fractionation factors are then combined to derive a value for the mineral–rock oxygen isotope fractionation. For the Grønnedal-Ika nepheline syenites at 800°C, $\Delta_{cpx-rock}$ is −1·1‰. $\delta^{18}O_{melt}$ for the gabbroic xenolith was calculated using $\Delta_{diopside-rock} = -0{\cdot}7$‰, based on the gabbro–water fractionation of Zhao & Zheng (2003) at 1000°C. The overall error introduced by uncertainties in mineral composition and T_{eq} is estimated to be <0·4‰ and does not affect the conclusions.

Results for the syenitic melts yield an average $\delta^{18}O$ value of 5·7 ± 0·3‰ with a range from 5·3 to 6·3‰ and 5·8‰ for the gabbroic xenolith (Fig. 12b). These values are indistinguishable from $\delta^{18}O$ melt compositions calculated for the EF basalts (5·5–6·3‰; Halama *et al.*, 2003), typical MORB glass compositions (5·37–5·81‰; Eiler *et al.*, 2000*b*) and unaltered whole-rock MORBs (5·7 ± 0·2‰; Harmon & Hoefs, 1995) and indicate a mantle derivation for the nepheline syenites with insignificant crustal contamination (Table 5, Fig. 12b). In comparison with $\delta^{18}O_{whole-rock}$ data from the Grønnedal-Ika syenites, which range from 8·3 to 15·1‰ (Pearce *et al.*, 1997), the calculated $\delta^{18}O_{melt}$ values are significantly lower and more homogeneous. In our view, the small scatter of

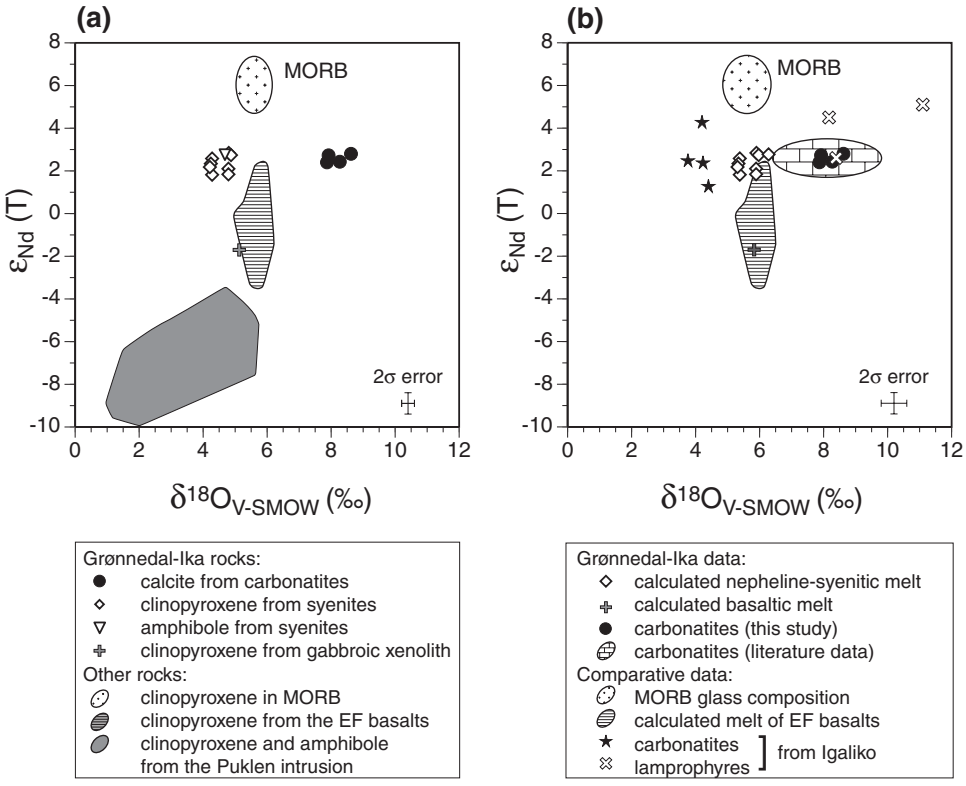

Fig. 12. Oxygen–neodymium isotope correlation diagrams for (a) mineral data and (b) calculated melt compositions and whole-rock analyses. ε_{Nd} ($T = 1{\cdot}3$ Ga) values for MORB were calculated using the DMM models of DePaolo (1981) and Goldstein *et al.* (1984). The hypothetical oxygen isotope composition of clinopyroxene in MORB was calculated based on analyses of MORB olivine ($\delta^{18}O = 5{\cdot}2$‰; Eiler *et al.*, 1997) and the oxygen isotope fractionation between olivine and clinopyroxene ($\Delta_{ol-cpx} = -0{\cdot}4$‰; Mattey *et al.*, 1994). Comparative mineral data are from Halama *et al.* (2003; EF basalts), Marks *et al.* (2003; Puklen intrusion) and Marks *et al.* (2004*b*; Ilímaussaq). For calculation of melt compositions, see text. MORB glass data are from Eiler *et al.* (2000*b*), comparative whole-rock data from Gardar rocks were taken from Pearce & Leng (1996; Igaliko dikes). The Grønnedal-Ika carbonatite field indicates available oxygen isotope data from various sources (Pearce *et al.*, 1997; Taubald *et al.*, 2004) combined with the Nd isotope data of this study.

the mineral oxygen isotope data compared with the whole-rock data suggests that the isotopic signatures in the minerals are primary, whereas the whole-rock data are suspected of having undergone late- to post-magmatic alteration. Products of late- to post-magmatic alteration are presumably concentrated along crystal boundaries, which are the parts of the sample removed during sample preparation for mineral analysis.

Carbon and oxygen isotope compositions of carbonatites

Based on the very small differences between measured whole-rock C and O isotope values and carbonate phenocrysts from the Oldoinyo Lengai volcano, Keller & Hoefs (1995) concluded that the isotopic fractionation between carbonate phenocrysts and residual melt is very small. Therefore, we can assume that $\delta^{13}C$ and $\delta^{18}O$ values in calcite are roughly equal to those in the carbonatite melt and thus comparable with the whole-rock data. This is confirmed by the overlap of published calcite and whole-rock compositions (Pearce *et al.*, 1997; Taubald *et al.*, 2004). The C and O isotope data are compatible with a primary magmatic, mantle-derived carbonatite (Fig. 8), i.e. largely unaffected by superficial secondary processes, although some minor late- to post-magmatic alteration is possible (Taubald *et al.*, 2004).

Carbonatitic dykes from the Igaliko dyke swarm have a larger range in $\delta^{18}O_{whole\text{-}rock}$ values (2·5–9·2‰; Pearce & Leng, 1996) than the Grønnedal carbonatites. However, the average of $4{\cdot}7 \pm 1{\cdot}5$‰ is significantly lower, possibly because of a high-T meteoric water influence (Fig. 8).

DISCUSSION

Carbonatite petrogenesis

In many cases, silica-undersaturated mantle melts contain carbonates (e.g. Riley *et al.*, 1996), and such magmas may exsolve an immiscible carbonate melt at crustal or

deeper levels (e.g. Freestone & Hamilton, 1980; Kjarsgaard, 1998) or potentially evolve towards carbonatitic compositions via extensive fractionation (e.g. Lee & Wyllie, 1994). Several alkaline complexes have been interpreted to contain such so-called primary carbonatites (Gittins, 1989). The term 'primary carbonatite' implies a near-solidus partial melt in equilibrium with CO_2-rich peridotitic mantle (Eggler, 1989). Primary carbonatites are characterized by elevated Mg-numbers (Sweeney, 1994), high (Mg + Fe)/Ca ratios, moderate amounts of alkalis (Eggler, 1989) and must have compositions dominated by calcic dolomite (Lee & Wyllie, 1998). This essentially excludes calciocarbonatites, as candidates for primary carbonatitic magmas and the whole-rock carbonatite data of Pearce *et al.* (1997) indicate that none of the Grønnedal-Ika samples satisfy these criteria because they are characterized by low amounts of MgO (<0·8 wt %) and alkalis (<0·5 wt %). Thus, the geochemical data do not favor a primary, unfractionated origin for the Grønnedal-Ika carbonatites. The syenites also do not have primary mantle–melt compositions, but compositions that indicate extensive crystal–liquid differentiation processes at crustal levels (Bühn & Trumbull, 2003).

Some experimental data (e.g. Lee & Wyllie, 1994) support a fractionation model for the genesis of carbonatites. However, the experimental residual liquids of carbonated alkali silicate melts were fairly silica-rich and not carbonatitic in composition, indicating that fractionation alone is not a feasible mechanism for generating carbonatites from alkali silicate melts at low pressures of 0·2 and 0·5 GPa (Kjarsgaard, 1998). Furthermore, fractionation alone cannot generate the Nb and REE concentrations characteristic of carbonatites (Srivastava, 1997). At Grønnedal-Ika, clinopyroxene is the principal mafic mineral in the syenites and its crystallization will reduce the CaO content in the remaining melt, thus inhibiting the formation of large amounts of calcite. There is also a suggestive lack of mineralogical and chemical continuity between the syenites and carbonatites at Grønnedal-Ika, which is inconsistent with a fractional crystallization relationship (Le Bas, 1989). Therefore, most arguments speak against an origin of the Grønnedal-Ika carbonatites solely by fractional crystallization.

Liquid immiscibility

Immiscible carbonate-rich magmas separated from silicate magmas tend to have calciocarbonatite compositions (Lee & Wyllie, 1998). The strongly SiO_2-undersaturated, peralkaline character of the Grønnedal-Ika nepheline syenites resembles the composition of the silicate liquids in early liquid immiscibility experiments (Koster van Groos & Wyllie, 1973). Based on the higher melt–solid interfacial energy of an immiscible carbonate melt compared with the coexisting silicate melt and the resulting restricted migration capability, Minarik (1998) argued that carbonatite should be the last phase in the temporal development of a syenite complex, which is clearly the case in Grønnedal-Ika.

Further support for liquid immiscibility comes from the overlap in $\varepsilon_{Nd}(T)$ values between the syenites and carbonatites (Table 6, Fig. 12). Published Sr isotope data also show similar initial $^{87}Sr/^{86}Sr$ ratios for the two rock types (Pearce *et al.*, 1997). Significant contamination with crustal material seems unlikely, as the local Archean gneiss country rock has strongly negative $\varepsilon_{Nd}(T)$ values that would cause a shift towards lower ε_{Nd}. The Nd isotope data show that the Grønnedal-Ika rocks are derived either from an isotopically slightly depleted (relative to Bulk Silicate Earth), homogeneous mantle source or a mixture of at least two mantle end-members, one isotopically depleted and one less depleted or enriched. The identical $\varepsilon_{Nd}(T)$ values of carbonatites and syenites would require melting of similar mantle end-members in the same proportions by different melting events, which is rather unlikely. Thus, the simplest explanation of the Nd isotope data is one involving magmatic differentiation. A liquid immiscibility origin between carbonatites and lamprophyres, as suggested by Pearce *et al.* (1997), has recently been re-evaluated by Coulson *et al.* (2003). Based on new geochemical data from the whole Gardar Province, they concluded, in agreement with previous work (Pearce & Leng, 1996; Pearce *et al.*, 1997), that carbonatitic and lamprophyric magmas were derived from the same mantle source, but explained differences between carbonatites and lamprophyres by differing degrees of partial melting of this source. The Nd isotope data from Grønnedal-Ika are in agreement with this conclusion and further suggest that the syenitic rocks are also derived from a similar source.

The oxygen isotopic fractionation between immiscible silicate and carbonate melts is unknown from direct experiments, but thought to be close to the fractionation between, for example, pyroxene and calcite (Santos & Clayton, 1995). At temperatures between 800 and 900°C, $\Delta_{calcite–cpx}$ varies between 1·0 for aegirine and 2·1 for diopside (Chiba *et al.*, 1989; Zheng, 1993*a*). Using these values and following the arguments above, we can roughly estimate the oxygen isotopic composition of the immiscible carbonatite melt from the calculated nepheline–syenitic melt composition of 5·7‰. It should be between 6·7 and 7·8‰, within the middle of the available $\delta^{18}O_{carbonatite\ melt}$ data (Fig. 12b). Thus, the oxygen isotope data are consistent with a petrogenetic model for the origin of the carbonatites involving liquid immiscibility. This is in contrast to the conclusion of Pearce *et al.* (1997), who argued that the difference in $\delta^{18}O$ values between the carbonatites and the whole-rock syenitic samples contradicts a liquid immiscibility origin.

Trace-element abundances in calcite

Experimental data on the partitioning of trace elements between immiscible carbonate and silicate liquids at 0·8 and 0·9 kbar (Veksler *et al.*, 1998*b*) can be used to evaluate whether certain trace-element characteristics of carbonatitic and syenitic calcite can be explained by this process. Types B and C calcite are not considered here because of their unusual chemistry and possible alteration. The similar patterns and relative enrichment levels of calcite from sample GM 1502 (type A) and the whole-rock carbonatites indicate that the relative enrichment of REE in the Grønnedal-Ika carbonatites is controlled by calcite (Fig. 5a). Type A calcite (sample GM 1502) is especially rich in Sr, Ba and P. These compositional features were also found in experimentally produced immiscible carbonatite liquids at low P ($\leq$0·5 kbar) by Kjarsgaard (1998), suggesting a similar origin for the Grønnedal carbonatites. These liquids were considered as good analogues for calciocarbonatites (Kjarsgaard, 1998), as they were also high in CaO and low in alkalis. The relatively high Ba contents of type A calcite compared with calcite from the syenites is in agreement with experimental partitioning data between silicate and carbonate melts that show a strong preference of Ba for the carbonate phase (Veksler *et al.*, 1998*b*). Negative Eu anomalies and lower Sr contents in calcite from the syenites are likely to be because of feldspar precipitation. The experimental data also indicate a relative preference of the LREE over the HREE for the carbonate liquid, which is qualitatively consistent with the higher La_{CN}/Yb_{CN} ratios in calcite from the carbonatite compared with calcite from the syenites. However, the high absolute REE concentrations in the carbonatites are difficult to reconcile with liquid immiscibility experiments, which show a preference for most REE in the silicate liquid (Veksler *et al.*, 1998*b*). Nevertheless, it was argued that the REE are preferentially partitioned into the carbonate liquids because the REE are preferentially transported by $(CO_3)^{2-}$- and F^--complexes that are more easily formed in carbonatitic liquids (Cullers & Medaris, 1977; Möller *et al.*, 1980). Additionally, whole-rock trace-element compositions of the syenites and carbonatites are also consistent with a petrogenetic origin involving liquid immiscibility (Bedford, 1989; Pearce *et al.*, 1997).

Crystallization of the nepheline syenites

Differences in the chemical and petrological evolution of alkali silicate complexes, with and without associated carbonatite, have previously been related to different CO_2 contents because of melt extraction from different mantle portions on a small scale or different degrees of melting (Bühn & Trumbull, 2003). Resulting compositional differences could be related to a process of silicate–carbonate liquid immiscibility (Bühn & Trumbull, 2003). Therefore, we will compare the petrology of the Grønnedal-Ika syenites with similar rocks from complexes of the Gardar Province that comprise no carbonatites (Fig. 1b), including silica-undersaturated rocks from Igdlerfigssalik (Powell, 1978), Ilímaussaq (Larsen, 1976; Marks & Markl, 2001; Markl *et al.*, 2001), South Qôroq (Stephenson, 1973), Motzfeldt (Jones, 1984) and silica-oversaturated rocks from the Puklen intrusion (Marks *et al.*, 2003).

T–aSiO_2–fO_2 conditions

In general, the Layered Syenites, the PMS and the matrix of the XPS equilibrated under very similar T–$a$$SiO_2$ conditions. The calculated silica activities of the Grønnedal-Ika syenites are distinctly lower than in similar rocks from other intrusive complexes of the Gardar Province not associated with carbonatites, such as the early augite syenite unit of Ilímaussaq ($a$$SiO_2$ = 0·4–0·9; Marks & Markl, 2001) and the syenitic rocks of Puklen ($a$$SiO_2$ = 0·7–1; Marks *et al.*, 2003). Oxygen fugacities during the early magmatic stage appear to be distinctly higher in Grønnedal-Ika than in syenitic rocks from Ilímaussaq (1–5 log units below FMQ; Marks & Markl, 2001), Igdlerfigssalik (2–3·5 log units below FMQ; Powell, 1978) and Puklen (1–3 log units below FMQ; Marks *et al.*, 2003). The almost complete absence of olivine and aenigmatite, which occurs in other Gardar complexes, and the differences in the onset of Na enrichment in clinopyroxenes (Fig. 3) is probably also related to differences in oxygen fugacity (Bedford, 1989). In the Ilímaussaq augite syenite, there is also no indication of more oxidizing conditions during late-magmatic stages (Marks & Markl, 2001) (Fig. 11). However, fO_2 increases during cooling relative to the FMQ buffer curve towards values above the HM buffer in the agpaitic magmas of Ilímaussaq (Markl *et al.*, 2001) as well as in syenitic and granitic magmas of Puklen (Marks *et al.*, 2003). These trends are similar to the one observed in the Grønnedal-Ika syenites.

Based on the argument that the silica-undersaturated character of mafic alkaline lavas can be attributed to low degrees of partial melting under CO_2-rich conditions (Mysen & Boettcher, 1975; Wyllie & Huang, 1976; Gerlach *et al.*, 1988), the very low silica activities of the Grønnedal-Ika syenites may indicate a high CO_2 content in the parental magmas which could increase during magma differentiation. Build-up of CO_2 is also indicated by the occurrence of calcite and cancrinite in the nepheline syenites. Further constraints on fCO_2 can be derived from the equilibrium $CH_4 + 2O_2 = CO_2 + 2H_2O$ at variable fCH_4/fCO_2 ratios in T–fO_2 space (Fig. 11). The reaction curve approaches conditions estimated for the Grønnedal syenites from the titanomagnetite compositions only for $fCH_4/fCO_2 < 0{\cdot}1$. This is consistent with the commonly observed dominance of CO_2–H_2O fluid inclusions in carbonatites (Andersen, 1986; Samson *et al.*,

1995; Bühn & Rankin, 1999). On the other hand, high fCH_4/fCO_2 ratios of >0·9 are indicated for the Ilímaussaq syenites, which is consistent with the presence of methane-bearing fluid inclusions with low CO_2 contents (Konnerup-Madsen & Rose-Hansen, 1982). A high fugacity of CO_2 would be an important prerequisite for carbonatite formation at Grønnedal-Ika and a different fCO_2 in the Grønnedal-Ika parental melt could be the most important difference from the Ilímaussaq parental melt.

Trace elements in clinopyroxene

A qualitative assessment of the trace-element patterns in the Grønnedal clinopyroxenes by comparison with clinopyroxenes from other Gardar complexes not associated with carbonatite reveals no significant differences in trace-element contents or patterns (Fig. 6b; Marks *et al.*, 2004*a*). It therefore appears that crystal-chemical effects dominate the trace-element partitioning behavior (Wood & Blundy, 1997; Blundy & Wood, 2003), and other effects, such as temperature and melt chemistry, play a subordinate role.

Ratios of geochemical twin elements, such as Zr/Hf and Y/Ho, can be used as petrogenetic indicators for comparing intrusions with and without associated carbonatites. Bühn & Trumbull (2003) found, for instance, significantly higher Zr/Hf ratios in syenitic rocks associated with carbonatite compared with ones without and related these differences to the ability of CO_2-rich fluids to fractionate Zr from Hf (Dupuy *et al.*, 1992; Irber, 1999). The Zr/Hf ratios in the clinopyroxene cores from the XPS overlap with those of other Grønnedal-Ika nepheline syenites (Zr/Hf = 31–43) and with those from augite syenitic units at Ilímaussaq (Zr/Hf = 29–34). The higher Zr/Hf ratios in the phenocryst rims are not likely to be because of fractionation of clinopyroxene, as both elements are mildly incompatible and the effect on Zr/Hf fractionation is negligible when only one ferromagnesian mineral is present (Linnen & Keppler, 2002). Experimental evidence also shows that there is little or no Zr/Hf fractionation in alkaline depolymerized melts (Linnen & Keppler, 2002). The lower Y/Ho ratios in phenocryst rims (Fig. 7) are consistent with exsolution of a CO_2-dominated fluid, which would leave the melts with successively decreasing Y/Ho ratios (Bühn & Trumbull, 2003). These differences in Zr/Hf and Y/Ho ratios suggest that clinopyroxene cores might have grown before, and rims during or after the separation of a CO_2-rich fluid. A pure crystal-chemical control on these trends seems unlikely because the major element compositions of clinopyroxene rims in the XPS and matrix clinopyroxene in the Layered Syenites are very similar.

SUMMARY AND CONCLUSIONS

The aim of the present study of the Grønnedal-Ika complex was to explore the relationship between the syenitic and carbonatitic rocks, to constrain the mode of origin of the carbonatite and to investigate what makes the syenitic rocks distinct from other Gardar complexes. We conclude that most of the available data indicate an origin of the carbonatite via liquid immiscibility from a parental silicate liquid. Criteria that support this model are listed below.

- Field and petrographic evidence suggests that there was no significant time gap between the emplacement of the silicate rocks and the carbonatites.
- Whole-rock and mineral geochemical fractionation indices such as Mg-number and $(Mg + Fe^{2+})/Ca$ confirm that the carbonatites do not represent unfractionated mantle melts. Clearly, the syenitic silicate rocks also crystallized from fractionated melts.
- Radiogenic isotope compositions (Sr: Pearce *et al.*, 1997; Nd: this study) are similar for silicate rocks and carbonatites.
- Oxygen isotope ratios for syenitic melts, determined from a set of mafic mineral data using appropriate fractionation factors between minerals and whole rocks (Zhao & Zheng, 2003), are in the range of typical mantle values ($\delta^{18}O = 5{\cdot}7‰$) and roughly 2‰ below the carbonatite melt values. This difference in $\delta^{18}O$ is within the range of theoretical expectations.
- In agreement with liquid immiscibility experiments (Veksler *et al.*, 1998*b*), the normalized REE patterns of calcite from carbonatites have steeper slopes than calcite from the associated silicate rocks. The same is true for carbonatite whole rocks compared with the syenites.
- The precipitation of aegirine–augitic clinopyroxene in the XPS with elevated Zr/Hf and lower Y/Ho ratios are consistent with effects that one would expect from the exsolution of a CO_2-rich fluid–melt. This may suggest that the XPS represents the conjugate silicate liquid in an immiscibility process.
- The silicate rocks associated with the carbonatites are strongly silica-undersaturated.
- The discreteness of occurrence favors liquid immiscibility rather than a fractional crystallization relationship in which continuous series of silicate to carbonate rocks would be expected (Le Bas, 1989).
- The carbonatites represent the latest phase in the complex (Minarik, 1998).

We conclude that the Grønnedal-Ika carbonatites are related via liquid immiscibility to the associated syenites. The syenites are characterized by relatively high fugacities of CO_2 and O_2 compared with other Gardar syenites not associated with carbonatites, which might explain the occurrence of carbonatite at Grønnedal-Ika. Some of the

data suggest that the xenolithic porphyritic syenite represents the conjugate silicate liquid.

ACKNOWLEDGEMENTS

We would like to acknowledge Henry Emeleus, Kathryn Goodenough and Robert Trumbull, as well as Marjorie Wilson for their constructive reviews, which greatly improved the paper. We are also grateful to Bruce Paterson, who provided invaluable help during laser ICP–MS measurements at the Large-Scale Geochemical Facility supported by the European Community–Access to Research Infrastructure action of the Improving Human Potential Programme, contract number HPRI-CT-1999–00008 awarded to Professor B. J. Wood (University of Bristol). Thanks to the courtesy of Kathryn Goodenough, Chris Bedford and Heinrich Taubald, we were able to include some of their unpublished data into this work. Additional thanks go to Chris Bedford for making available a copy of his voluminous Ph.D. thesis via Henry Emeleus. Gabi Stoschek, Bernd Steinhilber and Elmar Reitter expertly assisted with stable and radiogenic isotope measurements. Thanks go to Thomas Wenzel for his help with microprobe measurements and his critical comments that helped to improve the manuscript. Michael Marks is thanked for his pleasant company during fieldwork. The naval station at Grønnedal provided valuable logistical support. Financial funding of this work by the Deutsche Forschungsgemeinschaft (grant Ma-2135/1–2) is gratefully acknowledged.

REFERENCES

Andersen, T. (1986). Magmatic fluids in the Fen Carbonatite Complex, S.E. Norway: evidence of mid-crustal fractionation from solid and fluid inclusions in apatite. *Contributions to Mineralogy and Petrology* **93**, 491–503.

Andersen, T. (1997). Age and petrogenesis of the Qassiarsuk Carbonatite–Alkaline Silicate Volcanic Complex in the Gardar Rift, South Greenland. *Mineralogical Magazine* **61**, 499–513.

Armstrong, J. T. (1991). Quantitative elemental analysis of individual microparticles with electron beam instruments. In: Heinrich, K. F. J. & Newbury, D. E. (eds) *Electron Probe Quantitation*. New York: Plenum, pp. 261–315.

Bau, M. (1991). Rare-earth element mobility during hydrothermal and metamorphic fluid–rock interaction and the significance of the oxidation state of europium. *Chemical Geology* **93**, 219–230.

Bau, M. (1996). Controls on the fractionation of isovalent trace elements in magmatic and aqueous systems: evidence from Y/Ho, Zr/Hf, and lanthanide tetrad effect. *Contributions to Mineralogy and Petrology* **123**, 323–333.

Bau, M. & Möller, P. (1992). Rare earth element fractionation in metamorphogenic hydrothermal calcite, magnesite and siderite. *Mineralogy and Petrology* **45**, 231–246.

Bedford, C. M. (1989). The mineralogy, geochemistry and petrogenesis of the Grønnedal-Ika complex, South West Greenland. Ph.D. thesis, University of Durham.

Bell, K. (1998). Radiogenic isotope constraints on relationships between carbonatites and associated silicate rocks—a brief review. *Journal of Petrology* **39**, 1987–1996.

Bell, K., Kjarsgaard, B. A. & Simonetti, A. (1998). Carbonatites—into the twenty-first century. *Journal of Petrology* **39**, 1839–1845.

Berman, R. G., Brown, T. H. & Perkins, E. H. (1987). GEO–CALC: software for calculation and display of pressure–temperature–composition phase diagrams. *American Mineralogist* **72**, 861–862.

Blaxland, A. B., van Breemen, O., Emeleus, C. H. & Anderson, J. G. (1978). Age and origin of the major syenite centers in the Gardar Province of South Greenland: Rb–Sr studies. *Geological Society of America Bulletin* **89**, 231–244.

Blundy, J. & Wood, B. (2003). Partitioning of trace elements between crystals and melts. *Earth and Planetary Science Letters* **210**, 383–397.

Bondam, J. (1992). *The Grønnedal-Ika Alkaline Complex in South Greenland. Review of Geoscientific Data relevant to Exploration. Grønlands Geologiske Undersøgelse, Open File Series* **92**.

Boynton, W. V. (1984). Geochemistry of the rare earth elements: meteorite studies. In: Henderson, P. (ed.) *Rare Earth Element Geochemistry*. Amsterdam: Elsevier, pp. 63–114.

Brooker, R. (1998). The effect of CO_2 saturation on immiscibility between silicate and carbonate liquids: an experimental study. *Journal of Petrology* **39**, 1905–1915.

Buddington, A. F. & Lindsley, D. H. (1964). Iron–titanium oxide minerals and synthetic equivalents. *Journal of Petrology* **5**, 310–357.

Bühn, B. & Rankin, A. H. (1999). Composition of natural, volatile-rich Na–Ca–REE–Sr carbonatitic fluids trapped in fluid inclusions. *Geochimica et Cosmochimica Acta* **63**, 3781–3797.

Bühn, B. & Trumbull, R. B. (2003). Comparison of petrogenetic signatures between mantle-derived alkali silicate intrusives with and without associated carbonatite, Namibia. *Lithos* **66**, 201–221.

Callisen, K. (1943). Igneous Rocks of the Ivigtut Region, Greenland; Part 1, the Nepheline Syenites of the Grønnedal-Ika Area. *Meddelelser om Grønland* **131**(8), 74 pp.

Chiba, H., Chacko, T., Clayton, R. N. & Goldsmith, J. R. (1989). Oxygen isotope fractionations involving diopside, forsterite, magnetite, and calcite: application to geothermometry. *Geochimica et Cosmochimica Acta* **53**, 2985–2995.

Coulson, I. M., Goodenough, K. M., Pearce, N. J. G. & Leng, M. J. (2003). Carbonatites and lamprophyres of the Gardar Province—a 'window' to the Sub-Gardar Mantle? *Mineralogical Magazine* **67**, 855–872.

Cullers, R. L. & Medaris, G. Jr (1977). Rare earth elements in carbonatite and cogenetic alkaline rocks; examples from Seabrook Lake and Callander Bay, Ontario. *Contributions to Mineralogy and Petrology* **65**, 143–153.

Dalton, J. A. & Presnall, D. C. (1998). The continuum of primary carbonatitic–kimberlititc melt compositions in equilibrium with lherzolite: data from the system CaO–MgO–Al_2O_3–SiO_2–CO_2 at 6 GPa. *Journal of Petrology* **39**, 1953–1964.

Deines, P. (1989). Stable isotope variations in carbonatites. In: Bell, K. (ed.) *Carbonatites*.London: Unwin Hyman, pp. 301–359.

Demény, A., Ahijado, A., Casillas, R. & Vennemann, T. W. (1998). Crustal contamination and fluid/rock interaction in the carbonatites of Fuerteventura (Canary Islands, Spain): A C, O, H isotope study. *Lithos* **44**, 101–115.

DePaolo, D. J. (1981). Trace element and isotopic effects of combined wallrock assimilation and fractional crystallisation. *Earth and Planetary Science Letters* **53**, 189–202.

Dupuy, C., Liotard, J. M. & Dostal, J. (1992). Zr/Hf fractionation in intraplate basaltic rocks: carbonate metasomatism in the mantle source. *Geochimica et Cosmochimica Acta* **56**, 2417–2423.

Eggler, D. H. (1989). Carbonatites, primary melts, and mantle dynamics. In: Bell, K. (ed.) *Carbonatites*. London: Unwin Hyman, pp. 561–579.

Eiler, J. M., Farley, K. A., Valley, J. W., Hauri, E., Craig, H., Hart, S. R. & Stolper, E. M. (1997). Oxygen isotope variations in Ocean Island basalt phenocrysts. *Geochimica et Cosmochimica Acta* **61**, 2281–2293.

Eiler, J. M., Crawford, A., Elliot, T., Farley, K. A., Valley, J. W. & Stolper, E. M. (2000*a*). Oxygen isotope geochemistry of oceanic-arc lavas. *Journal of Petrology* **41**, 229–256.

Eiler, J. M., Schiano, P., Kitchen, N. & Stolper, E. M. (2000*b*). Oxygen-isotope evidence for recycled crust in the sources of mid-ocean-ridge basalts. *Nature* **403**, 530–534.

Emeleus, C. H. (1964). The Grønnedal-Ika alkaline complex, South Greenland. The structure and geological history of the complex. *Meddelelser om Grønland* **172**, 1–75.

Freestone, I. C. & Hamilton, D. L. (1980). The role of liquid immiscibility in the genesis of carbonatites—an experimental study. *Contributions to Mineralogy and Petrology* **73**, 105–117.

Fuhrman, M. L. & Lindsley, D. H. (1988). Ternary-feldspar modeling and thermometry. *American Mineralogist* **73**, 201–205.

Garde, A. A., Hamilton, M. A., Chadwick, B., Grocott, J. & McCaffrey, K. J. W. (2002). The Ketilidian Orogen of South Greenland: geochronology, tectonics, magmatism, and fore-arc accetion during Palaeoproterozoic oblique convergence. *Canadian Journal of Earth Sciences* **39**, 765–793.

Gerlach, D. C., Cliff, R. A., Davies, G. R., Norry, M. & Hodgson, N. (1988). Magma sources of the Cape Verdes Archipelago: isotopic and trace element constraints. *Geochimica et Cosmochimica Acta* **52**, 2979–2992.

Gill, R. C. O. (1972*a*). Chemistry of peralkaline phonolite dykes from the Grønnedal-Ika Area, South Greenland. *Contributions to Mineralogy and Petrology* **34**, 87–100.

Gill, R. C. O. (1972*b*). The geochemistry of the Grønnedal-Ika Alkaline Complex, South Greenland. Ph.D. thesis, University of Durham.

Gittins, J. (1989). The origin and evolution of carbonatite magmas. In: Bell, K. (ed.) *Carbonatites*. London: Unwin Hyman, pp. 580–600.

Gittins, J. & Harmer, R. E. (1997). What is ferrocarbonatite? A revised classification. *Journal of African Earth Sciences* **25**, 159–168.

Goldstein, S. L., O'Nions, R. K. & Hamilton, P. J. (1984). A Sm–Nd isotopic study of the atmospheric dust and particulates from major river systems. *Earth and Planetary Science Letters* **70**, 221–236.

Goodenough, K. M. (1997). Geochemistry of gardar intrusions in the Ivigtut Area, South Greenland. Ph.D. thesis, University of Edinburgh.

Halama, R., Waight, T. & Markl, G. (2002). Geochemical and isotopic zoning patterns of plagioclase megacrysts in gabbroic dykes from the Gardar Province, South Greenland: implications for crystallisation processes in anorthositic magmas. *Contributions to Mineralogy and Petrology* **144**, 109–127.

Halama, R., Wenzel, T., Upton, B. G. J., Siebel, W. & Markl, G. (2003). A geochemical and Sr–Nd–O isotopic study of the Proterozoic Eriksfjord Basalts, Gardar Province, South Greenland: Reconstruction of an OIB signature in crustally contaminated rift-related basalts. *Mineralogical Magazine* **67**, 831–854.

Hamilton, D. L. (1961). Nephelines as crystallisation temperature indicators. *Journal of Geology* **69**, 321–329.

Harmer, R. E. (1999). The petrogenetic association of carbonatite and alkaline magmatism: constraints from the Spitskop Complex, South Africa. *Journal of Petrology* **40**, 525–548.

Harmer, R. E. & Gittins, J. (1998). The case for primary, mantle-derived carbonatite magma. *Journal of Petrology* **39**, 1895–1903.

Harmon, R. S. & Hoefs, J. (1995). Oxygen isotope heterogeneity of the mantle deduced from global ^{18}O systematics of basalts from different geotectonic settings. *Contributions to Mineralogy and Petrology* **120**, 95–114.

Holland, T. J. B. (1990). Activities of components in omphacitic solid solutions; an application of Landay theory of mixtures. *Contributions to Mineralogy and Petrology* **105**, 446–453.

Irber, W. (1999). The lanthanide tetrad effect and its correlation with K/Rb, Eu/Eu*, Sr/Eu, Y/Ho, and Zr/Hf of evolving peraluminous granites suites. *Geochimica et Cosmochimica Acta* **63**, 489–508.

Jones, A. P. (1984). Mafic silicates from the nepheline syenites of the Motzfeldt Centre, South Greenland. *Mineralogical Magazine* **48**, 1–12.

Kalamarides, R. I. (1986). High-temperature oxygen isotope fractionation among the phases of Kiglapait Intrusion, Labrador, Canada. *Chemical Geology* **58**, 303–310.

Keller, J. & Hoefs, J. (1995). Stable isotope characteristics of recent natrocarbonatites from Oldoinyo Lengai. In: Bell, K. & Keller, J. (eds) *Carbonatite Volcanism: Oldoinyo Lengai and the Petrogenesis of Natrocarbonatites*. Berlin: Springer, pp. 113–123.

Kjarsgaard, B. A. (1998). Phase relations of a carbonated high-CaO nephelinite at 0·2 and 0·5 GPa. *Journal of Petrology* **39**, 2061–2075.

Kjarsgaard, B. A. & Hamilton, D. L. (1988). Liquid immiscibility and the origin of alkali-poor carbonatites. *Mineralogical Magazine* **52**, 43–55.

Konnerup-Madsen, J. & Rose-Hansen, J. (1982). Volatiles associated with alkaline igneous rift activity: fluid inclusions in the Ilimaussaq Intrusion and the Gardar Granitic Complexes (South Greenland). *Chemical Geology* **37**, 79–93.

Konnerup-Madsen, J. & Rose-Hansen, J. (1984). Composition and significance of fluid inclusions in the Ilimaussaq Peralkaline Granite, South Greenland. *Bulletin de Minéralogie* **107**, 317–326.

Korobeinikov, A. N., Mitrofanov, F. P., Gehör, S., Laajoki, K., Pavlov, V. P. & Mamontov, V. P. (1998). Geology and copper sulphide mineralization of the Salmagorskii Ring Igneous Complex, Kola Peninsula, NW Russia. *Journal of Petrology* **39**, 2033–2041.

Koster van Groos, A. F. & Wyllie, P. J. (1973). Liquid immiscibility in the join $NaAlSi_3O_8$–$CaAlSi_2O_8$–Na_2CO_3–H_2O. *American Journal of Science* **273**, 465–487.

Larsen, L. M. (1976). Clinopyroxenes and coexisting mafic minerals from the alkaline Ilimaussaq intrusion, South Greenland. *Journal of Petrology* **17**, 258–290.

Le Bas, M. J. (1989). Diversification of carbonatite. In: Bell, K. (ed.) *Carbonatites*. London: Unwin Hyman, pp. 428–447.

Lee, W.-J. & Wyllie, P. J. (1994). Experimental data bearing on liquid immiscibility, crystal fractionation, and the origin of calciocarbonatites and natrocarbonatites. *International Geology Review* **36**, 797–819.

Lee, W.-J. & Wyllie, P. J. (1998). Petrogenesis of carbonatite magmas from mantle to crust, constrained by the system CaO–(MgO+FeO*)–(Na_2O+K_2O)–(SiO_2+Al_2O_3+TiO_2)–CO_2. *Journal of Petrology* **39**, 495–517.

Lieberman, J. & Petrakakis, K. (1991). TWEEQU thermobarometry, analysis of uncertainties and applications to granulites from Western Alaska. *Canadian Mineralogist* **29**, 857–887.

Linnen, R. L. & Keppler, H. (2002). Melt composition control of Zr/Hf fractionation in magmatic processes. *Geochimica et Cosmochimica Acta* **66**, 3293–3301.

Markl, G., Marks, M., Schwinn, G. & Sommer, H. (2001). Phase equilibrium constraints on intensive crystallization parameters of

the Ilimaussaq Complex, South Greenland. *Journal of Petrology* **42**, 2231–2258.

Marks, M. & Markl, G. (2001). Fractionation and assimilation processes in the alkaline augite syenite unit of the Ilimaussaq intrusion, South Greenland, as deduced from phase equilibria. *Journal of Petrology* **42**, 1947–1969.

Marks, M., Vennemann, T., Siebel, W. & Markl, G. (2003). Quantification of magmatic and hydrothermal processes in a peralkaline syenite–alkali granite complex based on textures, phase equilibria, and stable and radiogenic isotopes. *Journal of Petrology* **44**, 1247–1280.

Marks, M., Halama, R., Wenzel, T. & Markl, G. (2004*a*). Trace element variations in clinopyroxene and amphibole from alkaline to peralkaline syenites and granites: implications for mineral–melt trace element partitioning. *Chemical Geology* (in press).

Marks, M., Vennemann, T., Siebel, W. & Markl, G. (2004*b*). Nd-, O-, and H-isotopic evidence for complex, closed-system fluid evolution in the peralkaline Ilímaussaq Intrusion, South Greenland. *Geochimica et Cosmochimica Acta* **68**, 3379–3395.

Mattey, D., Lowry, D. & Macpherson, C. (1994). Oxygen isotope composition of mantle peridotite. *Earth and Planetary Science Letters* **128**, 231–241.

McDonough, W. F. & Sun, S. S. (1995). The composition of the Earth. *Chemical Geology* **120**, 223–253.

Minarik, W. G. (1998). Complications to carbonate melt mobility due to the presence of an immiscible silicate melt. *Journal of Petrology* **39**, 1965–1973.

Möller, P., Morteani, G. & Schley, F. (1980). Discussion of REE distribution patterns of carbonatites and alkalic rocks. *Lithos* **13**, 171–179.

Moore, K. R. & Wood, B. J. (1998). The transition from carbonate to silicate melts in the CaO–MgO–SiO_2–CO_2 system. *Journal of Petrology* **39**, 1943–1951.

Morimoto, N., Fabrie, J., Ferguson, A. K., Ginzburg, I. V., Ross, M., Seifert, F. A., Zussman, J., Aoki, K. & Gottardi, G. (1988). Nomenclature of pyroxenes. *Mineralogical Magazine* **52**, 535–550.

Mysen, B. O. & Boettcher, A. L. (1975). Melting of a hydrous mantle; ii, geochemistry of crystals and liquids formed by anatexis of mantle peridotite at high pressures and high temperatures as a function of controlled activities of water, hydrogen, and carbon dioxide. *Journal of Petrology* **16**, 549–593.

Pearce, N. J. G. & Leng, M. J. (1996). The origin of carbonatites and related rocks from the Igaliko Dyke Swarm, Gardar Province, South Greenland: field, geochemical and C–O–Sr–Nd isotope evidence. *Lithos* **39**, 21–40.

Pearce, N. J. G., Leng, M. J., Emeleus, C. H. & Bedford, C. M. (1997). The origins of carbonatites and related rocks from the Grønnedal-Ika Nepheline Syenite Complex, South Greenland: C–O–Sr isotope evidence. *Mineralogical Magazine* **61**, 515–529.

Powell, M. (1978). The crystallisation history of the Igdlerfigssalik Nepheline Syenite Intrusion, Greenland. *Lithos* **11**, 99–120.

Riley, T. R., Bailey, D. K. & Lloyd, F. E. (1996). Extrusive carbonatite from the Quaternary Rockeskyll Complex, West Eifel, Germany. *Canadian Mineralogist* **34**, 389–401.

Robie, R. A. & Hemingway, B. S. (1995). Thermodynamic properties of minerals and related substances at 298·15 K and 1 bar (105 Pascals) pressure and at higher temperatures. *US Geological Survey, Bulletin* **2131**, 461 pp.

Roddick, J. C., Sullivan, R. W. & Dudas, F. Ö. (1992). Precise calibration of Nd tracer isotopic composition for Sm–Nd studies. *Chemical Geology* **97**, 1–8.

Rumble, D. & Hoering, T. C. (1994). Analysis of oxygen and sulfur isotope ratios in oxide and sulfide minerals by spot heating with a carbon dioxide laser in a fluorine atmosphere. *Accounts of Chemical Research* **27**, 237–241.

Samson, I. M., Williams-Jones, A. E. & Liu, W. (1995). The chemistry of hydrothermal fluids in carbonatites: evidence from leachate and SEM-decrepitate analysis of fluid inclusions from Oka, Quebec, Canada. *Geochimica et Cosmochimica Acta* **59**, 1979–1989.

Santos, R. V. & Clayton, R. N. (1995). Variations of oxygen and carbon isotopes in carbonatites: a study of Brazilian alkaline complexes. *Geochimica et Cosmochimica Acta* **59**, 1339–1352.

Sharp, Z. D. (1990). A laser-based microanalytical method for the in-situ determination of oxygen isotope ratios of silicates and oxides. *Geochimica et Cosmochimica Acta* **54**, 1353–1357.

Sirbescu, M. & Jenkins, D. M. (1999). Experiments on the stability of cancrinite in the system Na_2O–CaO–Al_2O_3–SiO_2–CO_2–H_2O. *American Mineralogist* **84**, 1850–1860.

Sobolev, V. S., Bazarova, T. Y. & Kostyuk, V. P. (1974). Inclusions in the minerals of some types of alkaline rocks. In: Sørensen, H. (ed.) *The Alkaline Rocks*. London: John Wiley, pp. 389–401.

Spötl, C. & Vennemann, T. W. (2003). Continuous-flow isotope ratio mass spectrometric analysis of carbonate minerals. *Rapid Communications in Mass Spectrometry* **17**, 1004–1006.

Srivastava, R. K. (1997). Petrology, geochemistry and gensis of rift-related carbonatites of Ambadungar, India. *Mineralogy and Petrology* **61**, 47–66.

Stephenson, D. (1973). The petrology and mineralogy of the South Qôroq Centre, Igaliko Complex, South Greenland. Ph.D. thesis, University of Durham.

Sweeney, R. J. (1994). Carbonatite melt compositions in the Earth's mantle. *Earth and Planetary Science Letters* **128**, 259–270.

Taubald, H., Morteani, G. & Satir, M. (2004). Geochemical and isotopic (Sr, C, O) data from the alkaline complex of Grønnedal-Ika (South Greenland): evidence for unmixing and crustal contamination. *International Journal of Earth Sciences* **93**, 348–360.

Taylor, H. P., Frechen, J. & Degens, E. T. (1967). Oxygen and carbon isotope studies of carbonatites from the Laacher See District, West Germany and the Alnö District, Sweden. *Geochimica et Cosmochimica Acta* **31**, 407–430.

Upton, B. G. J., Emeleus, C. H., Heaman, L. M., Goodenough, K. M. & Finch, A. (2003). Magmatism of the Mid-Proterozoic Gardar Province, South Greenland: chronology, petrogenesis and geological setting. *Lithos* **68**, 43–65.

Veksler, I. V., Nielsen, T. F. D. & Sokolov, S. V. (1998*a*). Mineralogy of crystallized melt inclusions from Gardiner and Kovdor ultramafic alkaline complexes: implications for carbonatite genesis. *Journal of Petrology* **39**, 2015–2031.

Veksler, I. V., Petibon, C., Jenner, G. A., Dorfman, A. M. & Dingwell, D. B. (1998*b*). Trace element partitioning in immiscible silicate–carbonate liquid systems: an initial experimental study using a centrifuge autoclave. *Journal of Petrology* **39**, 2095–2104.

Vroon, P. Z., Lowry, D., Van Bergen, M. J., Boyce, A. J. & Mattey, D. P. (2001). Oxygen isotope systematics of the Banda Arc: low $\delta^{18}O$ despite involvement of subducted continental material in magma genesis. *Geochimica et Cosmochimica Acta* **65**, 589–609.

Wilkinson, J. F. G. & Hensel, H. D. (1994). Nephelines and analcimes in some alkaline igneous rocks. *Contributions to Mineralogy and Petrology* **118**, 79–91.

Wood, B. J. & Blundy, J. D. (1997). A predictive model for rare earth element partitioning between clinopyroxene and anhydrous silicate melt. *Contributions to Mineralogy and Petrology* **129**, 166–181.

Woolley, A. R. & Kempe, D. R. C. (1989). Carbonatites: nomenclature, average chemical compositions, and element distribution. In: Bell, K. (ed.) *Carbonatites*. London: Unwin Hyman, pp. 1–14.

Wyllie, P. J. & Huang, W. L. (1976). Carbonation and melting relations in the system CaO–MgO–SiO_2–CO_2 at mantle pressures with geophysical and petrological applications. *Contributions to Mineralogy and Petrology* **54**, 79–107.

Zhao, Z.-F. & Zheng, Y.-F. (2003). Calculation of oxygen isotope fractionation in magmatic rocks. *Chemical Geology* **193**, 59–80.

Zheng, Y.-F. (1993*a*). Calculation of oxygen isotope fractionation in anydrous silicate minerals. *Geochimica et Cosmochimica Acta* **57**, 1079–1091.

Zheng, Y.-F. (1993*b*). Calculation of oxygen isotope fractionation in hydroxyl-bearing silicates. *Earth and Planetary Science Letters* **120**, 247–263.